Articles

ATHENS INSTITUTE FOR EDUCATION AND RESEARCH
A World Association of Academics and Researchers
8 Valaoritou Str., Kolonaki, 10671 Athens, Greece.
Tel.: 210-36.34.210 Fax: 210-36.34.209
Email: info@atiner.gr URL: www.atiner.gr

(ATINER)   *Established in 1995*   *(ATINER)*

Mission

ATINER is a *World Non-Profit Association* of Academics and Researchers based in Athens. ATINER is an independent **Association** with a **Mission** to become a forum where Academics and Researchers from all over the world can meet in Athens, exchange ideas on their research and discuss future developments in their disciplines, **as well as engage with professionals from other fields**. Athens was chosen because of its long history of academic gatherings, which go back thousands of years to *Plato's Academy* and *Aristotle's Lyceum.* Both these historic places are within walking distance from ATINER's downtown offices. Since antiquity, Athens was an open city. In the words of Pericles, **Athens"...*is open to the world, we never expel a foreigner from learning or seeing".* (**"Pericles' Funeral Oration", in Thucydides, *The History of the Peloponnesian War).* It is ATINER's **mission** to revive the glory of Ancient Athens by inviting the World Academic Community to the city, to learn from each other in an environment of freedom and respect for other people's opinions and beliefs. After all, the free expression of one's opinion formed the basis for the development of democracy, and Athens was its cradle. As it turned out, the Golden Age of Athens was in fact, the Golden Age of the Western Civilization. *Education* and *(Re)searching* for the 'truth' are the pillars of any free (democratic) society. This is the reason why *Education* and *Research* are the two core words in ATINER's name.

Athens Journal of Technology & Engineering
Editorial and Reviewers' Board

President's Message

All ATINER's publications including the e-journals are open access without any costs (submission, processing, publishing, open access paid by authors, open access paid by readers etc.) and are independent of the presentations made at any of the many small events (conferences, symposiums, forums, colloquiums, courses, roundtable discussions) organized by ATINER throughout the year. The intellectual property rights of the submitted papers remain with the author.

Before you submit, please make sure your paper meets some basic academic standards, which include proper English. Some articles will be selected from the numerous papers that have been presented at the various annual international academic conferences organized by the different divisions and units of the Athens Institute for Education and Research.

The plethora of papers presented every year will enable the editorial board of each journal to select the best ones, and in so doing, to produce a quality academic journal. In addition to papers presented, ATINER encourages the independent submission of papers to be evaluated for publication.

The current issue of the Athens Journal of Technology & Engineering (AJTE) is the first issue of the sixth volume (2019). The reader will notice some changes compared with the previous issues, which I hope is an improvement. An effort has been made to include papers which extent to different fields of Technology and Engineering. Three papers are related to construction-structural engineering and one to human resource technologies.

Gregory T. Papanikos, President
Athens Institute for Education and Research

Athens Institute for Education and Research
A World Association of Academics and Researchers

9th Annual International Conference on Civil Engineering
24-27 June 2019, Athens, Greece

The Civil Engineering Unit of ATINER is organizing its **9th Annual International Conference on Civil Engineering, 24-27 June 2019, Athens, Greece** sponsored by the Athens Journal of Technology & Engineering. The aim of the conference is to bring together academics and researchers of all areas of Civil Engineering other related areas. You may participate as stream leader, presenter of one paper, chair of a session or observer. Please submit a proposal using the form available (https://www.atiner.gr/2019/FORM-CIV.doc).

Academic Members Responsible for the Conference

- **Dr. Dimitrios Goulias**, Head, Civil Engineering Unit, ATINER and Associate Professor & Director of Undergraduate Studies Civil & Environmental Engineering Department, University of Maryland, USA.

Important Dates
- Abstract Submission: **25 February 2019**
- Acceptance of Abstract: 4 Weeks after Submission
- Submission of Paper: **27 May 2019**

Social and Educational Program
The Social Program Emphasizes the Educational Aspect of the Academic Meetings of Atiner.
- Greek Night Entertainment (This is the official dinner of the conference)
- Athens Sightseeing: Old and New-An Educational Urban Walk
- Social Dinner
- Mycenae Visit
- Exploration of the Aegean Islands
- Delphi Visit
- Ancient Corinth and Cape Sounion

Conference Fees

Conference fees vary from 400€ to 2000€
Details can be found at: https://www.atiner.gr/2019fees

Athens Institute for Education and Research
A World Association of Academics and Researchers

7th Annual International Conference on Industrial, Systems and Design Engineering, 24-27 June 2019, Athens, Greece

The Industrial Engineering Unit of ATINER will hold its **7th Annual International Conference on Industrial, Systems and Design Engineering, 24-27 June 2019, Athens, Greece** sponsored by the Athens Journal of Technology & Engineering.The aim of the conference is to bring together academics, researchers and professionals in areas of Industrial, Systems, Design Engineering and related subjects. You may participate as stream leader, presenter of one paper, chair of a session or observer. Please submit a proposal using the form available (https://www.atiner.gr/2019/FORM-IND.doc).

Important Dates
- Abstract Submission: **25 February 2019**
- Acceptance of Abstract: 4 Weeks after Submission
- Submission of Paper: **27 May 2019**

Academic Member Responsible for the Conference

- **Dr. Theodore Trafalis**, Director, Engineering & Architecture Division, ATINER, Professor of Industrial & Systems Engineering and Director, Optimization & Intelligent Systems Laboratory, The University of Oklahoma, USA.

Social and Educational Program
The Social Program Emphasizes the Educational Aspect of the Academic Meetings of Atiner.
- Greek Night Entertainment (This is the official dinner of the conference)
- Athens Sightseeing: Old and New-An Educational Urban Walk
- Social Dinner
- Mycenae Visit
- Exploration of the Aegean Islands
- Delphi Visit
- Ancient Corinth and Cape Sounion
  More information can be found here: https://www.atiner.gr/social-program

Conference Fees
Conference fees vary from 400€ to 2000€
Details can be found at: https://www.atiner.gr/2019fees

Bending Analysis of Castellated Beams

By Sahar Elaiwi[*]
Boksun Kim[‡]
Long-Yuan Li[†]

Existing studies have shown that the load-carrying capacity of castellated beams can be influenced by the shear stresses particularly those around web openings and under the T-section, which could cause the beam to have different failure modes. This paper investigates the effect of web openings on the transverse deflection of castellated beams by using both analytical and numerical methods and evaluates the shear-induced transverse deflection of castellated beams of different lengths and flange widths subjected to uniformly distributed transverse load. The purpose of developing analytical solutions, which adopted the classical principle of minimum potential energy is for the design and practical use; while the numerical solutions are developed by using the commercial software ANSYS for the validation of the analytical solutions.

Keywords: *Castellated Beam, Deflection, Energy Method, Finite Element, Shear Effect.*

Introduction

Engineers and researchers have tried various methods to reduce the material and construction costs to help optimise the use of the steel structural members. The castellated beam is one of the steel members which uses less material, but has comparable performance as the I-beam of the same size (Altifillisch et al. 1957). An example is shown in Figure 1a. The castellated beam is fabricated from a standard universal I-beam or H-column by cutting the web on a half hexagonal line down the centre of the beam. The two halves are moved across by a half unit of spacing and then re-joined by welding. This process increases the depth of the beam and thus the bending strength and stiffness of the beam about the major axis are also enhanced without additional materials being added. This allows castellated beams to be used in long span applications with light or moderate loading conditions for supporting floors and roofs. In addition, the fabrication process creates openings on the web, which can be used to accommodate services. As a result, the designer does not need to increase the finished floor level. Thus, despite the increase in the beam depth the overall building height may actually be reduced.

When compared with a solid web solution where services are provided beneath the beam, the use of castellated beams could lead to savings in the cladding costs especially in recent years, the steel cost becomes higher. Owing to the fact that the steel materials have poor fire resistance, buildings made from steel

---
[*]PhD Student, Plymouth University, UK.
[‡]Plymouth University, UK.
[†]Plymouth University, UK.

structures require to use high quality fireproof materials to protect steel members from fire, which further increase its cost. Moreover, because of its lightweight the castellated beam is more convenient in transportation and installation than the normal I-beam.

Literature Review

For many years, the castellated beam have been used in construction because of its advantages when considering both the safety and serviceability while considering functional requirements according to the use for which the construction is intended. Extensive study has been done by researchers who are working in the construction field to identify the behaviour of castellated beams when they are loaded with different types of loads. It was found that the castellated beam could fail in various different modes depending on the dimensions of the beam and the type of loading as well as the boundary conditions of the beams. Kerdal and Nethercot (1984) informed the potential failure modes, which possibly take place in castellated beams. Also, they explained the reasons for the occurrence of these failure modes. For instance, shear force and web weld rupture cause a Vierendeel mechanism and web post-buckling. Additionally, they pointed out that any other failures whether caused by a flexural mechanism or a lateral-torsional instability is identical to the equivalent modes for beams without web opening.

The web openings in the castellated beam, however, may reduce the shear resistance of the beam. The saved evidence, that the method of analysis and design for the solid beam may not be suitable for the castellated beam (Boyer 1964, Kerdal and Nethercot 1984, Demirdjian 1999). Design guidance on the strength and stiffness for castellated beams is available in some countries. However, again, most of them do not take into account the shear effect. As far as the bending strength is concerned, neglecting the shear effect may not cause problems. However, for the buckling and the calculation of serviceability, the shear weakness due to web openings in castellated beams could affect the performance of the beams and thus needs to be carefully considered.

Experimental investigations (Aminian et al. 2012, Maalek 2004, Yuan et al. 2014, Yuan et al. 2016, Zaarour and Redwood, 1996) were carried out and finite elements methods (Hosain et al. 1974, Sherbourne and Van Oostrom 1972, Soltani et al. 2012, Sonck et al. 2015, Srimani and Das 1978, Wang et al. 2014) were also used to predict the deflection of castellated beams and/or to compare the predictions with the results from the experiments. The experimental findings (Zaarour and Redwood 1996) demonstrated the possibility of the occurrence of the buckling of the web posts between web openings. The shear deflection of the straight-sided tapering cantilever of the rectangular cross section (Maalek 2004) was calculated by using a theoretical method based on Timoshenko's beam theory and virtual work method. Linear genetic programming and integrated search algorithms (Aminian et al. 2012) showed that the use of the machine learning system is an active method to validate the failure load of castellated beams. A

numerical computer programme (Sherbourne and Van Oostrom 1972) was developed for the analysis of castellated beams considering both elastic and plastic deformations by using practical lower limit relationships for shear, moment and axial force interaction of plasticity. An analysis on five experimental groups of castellated beams (Srimani and Das 1978) was conducted to determine the deflection of the beam. It was demonstrated (Hosain et al. 1974) that the finite elements method is a suitable method for calculating the deflection of symmetrical section castellated beams. The effect of nonlinearity in material and/or geometry on the failure model prediction of castellated beams (Soltani et al. 2012) was done by using MSC/NASTRAN software to find out bending moments and shear load capacity, which are compared with those published in literature.

Axial compression buckling of castellated columns was investigated (Yuan et al. 2014), in which an analytical solution for critical load is derived based on stationary potential energy and considering the effect of the web shear deformations on the flexural buckling of simply supported castellated column. Recently, a parametric study on the large deflection analysis of castellated beams at high temperatures (Wang et al. 2014) was conducted by using finite element method to calculate the growth of the end reaction force, the middle span deflection, and the bending moments at susceptible sections of castellated beams. More recently, a comprehensive comparison between the deflection results of cellular and castellated beams obtained from numerical analysis (Sonck et al. 2015) was presented, which was obtained from different simplified design codes. The comparison showed that the design codes are not accurate for short span beams and conservative for long span beams. The principle of minimum potential energy was adopted (Yuan et al. 2016) to derive an analytical method to calculate the deflection of castellated/cellular beams with hexagonal/circular web openings, subjected to a uniformly distributed transverse load.

The previous research efforts show that there were a few of articles that dealt with the deflection analysis of castellated beams. Due to the geometric particulars of the beam, however, it was remarkable to note that most of the theoretical approximate methods are interested in calculating the deflection of the castellated beams for long span beams where the shear effect is negligible. However, the castellated beams/columns are used not only for long span beams/columns but also for short beams/columns. Owing to the complex of section profile of the castellated beams, the shear-effect caused by the web opening on the deflection calculation is not fully understood. There are no accurate calculation methods available in literature to perform these analyses. Thus it is important to know how the shear affects the deflection of the beam and on what kind of spans the shear effect can be ignored. In addition, researchers have adopted the finite elements method to predict the deflection of castellated beams by using different software programs such as MSC/NASTRAN, ABAQUS, and ANSYS. However, these programs need efficiency in use because any error could lead to significant distortions in results. European building standards do not have formulas for the calculation of deflections of castellated beams, which include shear deformations.

This paper presents the analytical method to calculate the elastic deflection of castellated beams. The deflection equation is to be developed based on the

principle of minimum potential energy. In order to improve the accuracy and efficiency of this method, shear rigidity factor is determined by using suitable numerical techniques. The analytical results were validated by using the numerical results obtained from the finite element analysis using ANSYS software.

Analytical Philosophy of Deflection Analysis of Castellated Beams

An approximate method of deflection analysis of castellated beams under a uniformly distributed transverse load is presented herein. The method is derived based on the principle of minimum potential energy of the structural system. Because of the presence of web openings, the cross-section of the castellated beam is now decomposed into three parts to calculate the deflection and bending stress, two of which represent the top and bottom T-sections, one of which represents the mid-part of the web. The analysis model is illustrated in Figure 1a, in which the flange width and thickness are b_f and t_f, the web depth and thickness are h_w and t_w, and the half depth of hexagons is a. The half of the distance between the centroids of the two T-sections is e. In this study, the cross-section of the castellated beam is assumed to be doubly symmetrical. Under the action of a uniformly distributed transverse load, the beam section will have axial and transverse displacement as shown in Figure 1b, where x is the longitudinal coordinate of the beam, z is the cross-sectional coordinate of the beam, (u_1, w) and (u_2, w) are the axial displacements and the transverse displacements of the centroids of the upper and lower T-sections. All points on the section are assumed to have the same transverse displacement because of the beam assumption used in the present approach (Yuan et al. 2014). The corresponding axial strains ε_{1x} in the upper T-section and ε_{2x} i in the lower T-section are linearly distributed and can be determined by using the strain-displacement relation as follows:

In the upper T-section: $-\left(\frac{h_w}{2} + t_f\right) \leq z \leq -a$

$$\varepsilon_{1x}(x,z) = \frac{du_1}{dx} - (z + e)\frac{d^2w}{dx^2} \tag{1}$$

In the lower T-section: $a \leq z \leq \left(\frac{h_w}{2} + t_f\right)$

$$\varepsilon_{2x}(x,z) = \frac{du_2}{dx} - (z - e)\frac{d^2w}{dx^2} \tag{2}$$

The shear strain γ_{xz} in the middle part between the two T-sections can also be determined using the shear strain-displacement relation as follows:

For the middle part between the two T-sections: $-a \leq z \leq a$

$$\gamma_{xz}(x,z) = \frac{du}{dz} + \frac{dw}{dx} = -\frac{u_1 - u_2}{2a} + \frac{e}{a}\frac{dw}{dx} \tag{3}$$

$$e = \frac{b_f t_f \left(\frac{h_w + t_f}{2}\right) + t_w \left(\frac{h_w}{2} - a\right)\left(\frac{h_w + 2a}{4}\right)}{b_f t_f + t_w \left(\frac{h_w}{2} - a\right)} \tag{4}$$

Because the upper and lower T-sections behave according to Bernoulli's theory, the strain energy of the upper T-section U_1 and the lower T-section U_2 caused by a transverse load can be expressed as follows:

$$U_1 = \frac{E b_f}{2} \int_0^l \int_{-(t_f + \frac{h_w}{2})}^{-\frac{h_w}{2}} \varepsilon_{1x}^2 \, dz \, dx + \frac{E t_w}{2} \int_0^l \int_{-(\frac{h_w}{2})}^{-a} \varepsilon_{1x}^2 \, dz \, dx$$

$$= \frac{1}{2} \int_0^l \left[EA_{tee} \left(\frac{du_1}{dx}\right)^2 + EI_{tee} \left(\frac{d^2 w}{dx^2}\right)^2 \right] dx \tag{5}$$

$$U_2 = \frac{E t_w}{2} \int_0^l \int_a^{(\frac{h_w}{2})} \varepsilon_{2x}^2 \, dz \, dx + \frac{E b_f}{2} \int_0^l \int_{\frac{h_w}{2}}^{(t_f + \frac{h_w}{2})} \varepsilon_{2x}^2 \, dz \, dx$$

$$= \frac{1}{2} \int_0^l \left[EA_{tee} \left(\frac{du_2}{dx}\right)^2 + EI_{tee} \left(\frac{d^2 w}{dx^2}\right)^2 \right] dx \tag{6}$$

where E is the Young's modulus of the two T-sections, G is the shear modulus, A_{tee} and I_{tee} are the area and the second moment of area of the T- section, which are determined in their own coordinate systems as follows:

$$A_{tee} = b_f t_f + t_w \left(\frac{h_w}{2} - a\right) \tag{7}$$

$$I_{tee} = \frac{b_f t_f^3}{12} + b_f t_f \left(\frac{h_w + t_f}{2} - e\right)^2 + \frac{t_w}{12} \left(\frac{h_w}{2} - a\right)^3$$

$$+ t_w \left(\frac{h_w}{2} - a\right)\left(\frac{h_w + 2a}{4} - e\right)^2 \tag{8}$$

The mid-part of the web of the castellated beam, which is illustrated in Figure 1a, is assumed to behave according to Timoshenko's theory (Yuan et al. 2014). Therefore, its strain energy due to the bending and shear can be expressed as follows:

$$U_b = \frac{1}{2} \sum K_b \, \Delta^2 \tag{9}$$

where Δ is the relative displacement of the upper and lower T-sections due to a pair of shear forces and can be expressed as ($\Delta = 2a\gamma_{xz}$). While K_b is the

combined stiffness of the mid part of the web caused by the bending and shear, and is determined in terms of Timoshenko beam theory as follows,

$$\frac{1}{K_b} = \frac{3l_b}{2GA_b} + \frac{l_b^3}{12EI_b} \tag{10}$$

where $A_b = \sqrt{3}at_w$ is the equivalent cross-sectional area of the mid part of the web, $I_b = (\sqrt{3}a)^3 t_w/12$ is the second moment of area, and $l_b = 2a$ is the length of the Timoshenko beam; herein representing the web post length. Note that, the Young's modulus of the two T-sections is $E = 2(1+v)G$ and the Poisson's ratio is taken as $v = 0.3$, the value of the combined stiffness of the mid part of the web caused by the bending and shear can be determined as fallow:

$$K_b = \frac{\sqrt{3}Gt_w}{4} \tag{11}$$

Thus, the shear strain energy of the web, U_{sh}, due to the shear strain γ_{xy} can be calculated as follows:

$$U_{sh} = \frac{\sqrt{3}}{2}Gt_w a^2 \sum_{k=1}^{n} \gamma_{xz}^2 \approx \frac{\sqrt{3}Gt_w a^2}{2 \times \frac{6a}{\sqrt{3}}} \int_0^l \gamma_{xz}^2 \, dx = \frac{Gt_w a}{4} \int_0^l \gamma_{xz}^2 \, dx \tag{12}$$

Let the shear rigidity factor $k_{sh} = 0.25$. Substituting Eqs. (3) into (12) gives the total shear strain energy of the mid-part of the web:

$$U_{sh} = \frac{Gt_w e^2 k_{sh}}{a} \int_0^l \left(\frac{dw}{dx} - \frac{u_\beta}{e}\right)^2 dx \tag{13}$$

Note that, in the calculation of shear strain energy of Eq. (12) one uses the concept of smear model, in which the shear strain energy was calculated first for web without holes. Then by assuming the ratio of the shear strain energies of the webs with and without holes is proportional to the volume ratio of the webs with and without holes, the shear strain energy of the web with holes was evaluated, in which $k_{sh} = 0.25$ was obtained (Kim et al. 2016). However, by using a two-dimensional linear finite element analysis (Yuan et al. 2016) the value of the combined stiffness of the mid part of the web of the castellated beam caused by the bending and shear, was found to be

$$K_b = 0.78 \times \frac{\sqrt{3}Gt_w}{4} \tag{14}$$

which is smaller than that above-derived from the smear model. This leads to

the shear rigidity factor k_{sh} = 0.78x0.25. The reason for this is probably due to the smear model used for the calculation of the shear strain energy for the mid-part of the web in Eq. (12).

Figure 1. (a) *Notations used in Castellated Beams* (b) *Displacements* and (c) *Internal Forces*
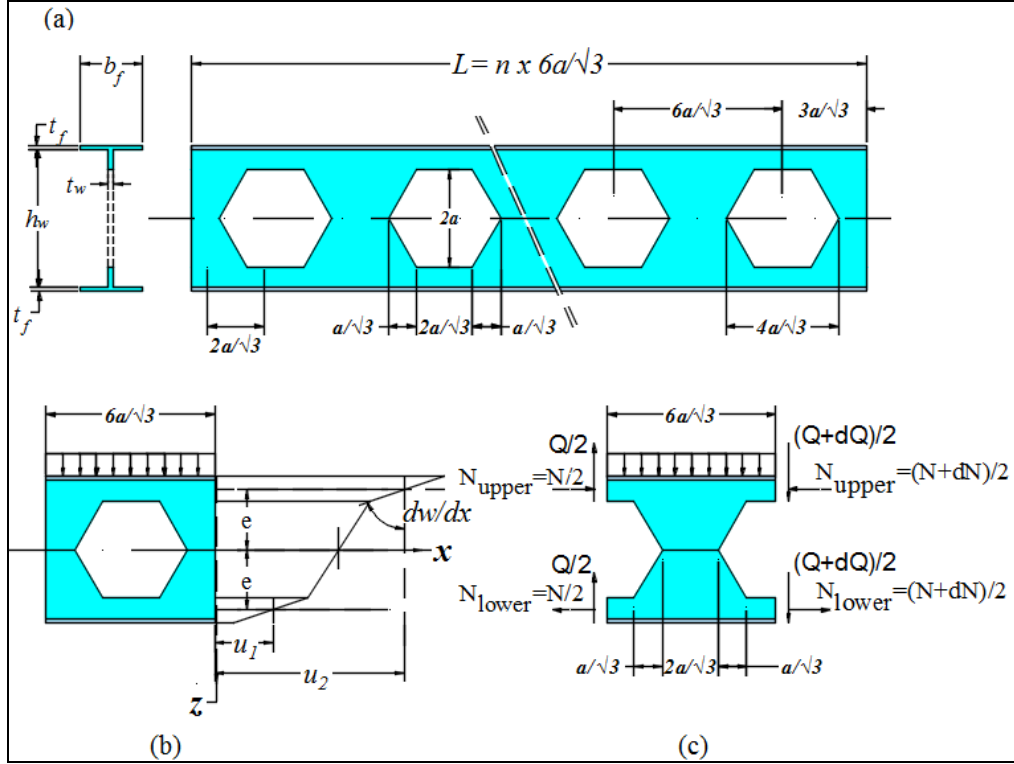
However, it should be mentioned that the factor of 0.78 in Eq. (14) was obtained for only one specific section of a castellated beam. It is not known whether this factor can also be applied to other dimensions of the beams. A finite element analysis model for determining the shear rigidity factor k_{sh} is therefore developed herein (see Figure 2c), in which the length and depth of the unit are (4a/√3) and (2a+a/2), respectively. In the unit the relative displacement Δ can be calculated numerically when a unit load *F* is applied (see Figure 2c). Hence, the combined rigidity K_b=1/Δ is obtained. Note that in the unit model all displacements and rotation of the bottom line are assumed to be zero, whereas the line where the unit load is applied is assumed to have zero vertical displacement. The calibration of the shear rigidity for beams of different section sizes shows that the use of the expression below gives the best results and therefore Eq. (15) is used in the present analytical solutions.

$$K_{sh} = \left(0.76 - \frac{b_f}{l}\right) \times \frac{1}{4} \tag{15}$$

where *l* is the length of the beam. Thus the total potential energy of the

castellated beam U_T is expressed as follows,

$$U_T = U_1 + U_2 + U_{sh} \tag{16}$$

For the simplicity of presentation, the following two new functions are introduced:

$$u_\alpha = \frac{u_1 + u_2}{2} \tag{17}$$

$$u_\beta = \frac{u_1 - u_2}{2} \tag{18}$$

By using Eqs. (17) and (18), the total potential energy of the castellated beam subjected to a uniformly distributed transverse load can be expressed as follows:

$$\Pi = EA_{tee} \int_0^l \left(\frac{du_\beta}{dx}\right)^2 dx + EI_{tee} \int_0^l \left(\frac{d^2w}{dx^2}\right)^2 dx$$
$$+ \frac{Gt_w e^2 k_{sh}}{a} \int_0^l \left(\frac{dw}{dx} - \frac{u_\beta}{e}\right)^2 dx - W \tag{19}$$

where W is the potential of the uniformly distributed load q_{max} due to the transverse displacement, which can be expressed as follows:

$$W = q_{max} \int_0^l w\, dx \tag{20}$$

where q_{max} is the uniformly distributed load, which can be expressed in terms of design stress σ_y, as follows:

$$q_{max} = 16 \frac{\sigma_y I_{reduced}}{l^2(h_w + 2t_f)} \tag{21}$$

$$I_{reduced} = \frac{b_f(h_w + 2t_f)^3}{12} - \frac{t_w a^3}{12} - \frac{(h_w)^3(b_f - t_w)}{12} \tag{22}$$

Figure 2. *Shear Strain Energy Calculation Model: (a) Unit Considered, (b) Shear Deformation Calculation Model and (c) Finite Element Model of 4a/√3 Length Unit and (2a+a/2) Depth, Loaded by a Unite Force F*
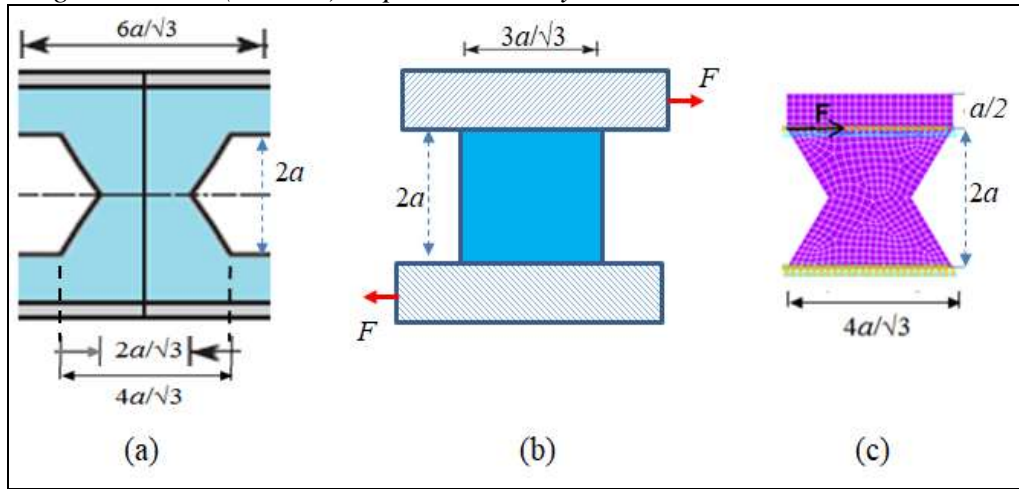
Deflection of Simply Supported Castellated Beam with Uniformly Distributed Transverse Loading

For a simply supported castellated beam $u_\alpha(x)$, $u_\beta(x)$ and $w(x)$ can be assumed as follows:

$$u_\alpha(x) = \sum_{m=1,2,..} A_m \cos\frac{m\pi x}{l} \tag{23}$$

$$u_\beta(x) = \sum_{m=1,2,..} B_m \cos\frac{m\pi x}{l} \tag{24}$$

$$w(x) = \sum_{m=1,2,..} C_m \sin\frac{m\pi x}{l} \tag{25}$$

where A_m, B_m and C_m are the constants to be determined. It is obvious that the displacement functions assumed in Eqs. (23)-(25) satisfy the simply support boundary conditions, that are $w = \frac{d^2 w}{dx^2} = 0$ and $\frac{du_\alpha}{dx} = \frac{du_\beta}{dx} = 0$ at $x = 0$ and $x = l$, and m = 1,2,… is the integral number. Substituting Eqs. (23), (24) and (25) into (19) and (20) and according to the principle of minimum potential energy, it yields,

$$\delta(U_T + U_{sh} - W) = 0 \tag{26}$$

The variation of Eq. (26) with respect to A_m, B_m and C_m results in following three algebraic equations:

$$EA_{tee}\left(\frac{m\pi x}{l}\right)^2 A_m = 0 \tag{27}$$

$$\left[EA_{tee}\left(\frac{m\pi}{l}\right)^2 + \frac{Gt_w k_{sh}}{a}\right]B_m - \left[\frac{Gt_w e k_{sh}}{a}\left(\frac{m\pi}{l}\right)\right]C_m = 0 \tag{28}$$

$$\left[EI_{tee}\left(\frac{m\pi}{l}\right)^4 + \frac{Gt_w e^2 k_{sh}}{a}\left(\frac{m\pi}{l}\right)^2\right]C_m - \left[\frac{Gt_w e k_{sh}}{a}\left(\frac{m\pi}{l}\right)\right]B_m$$
$$= \frac{[1-(-1)^m]q_{max}}{m\pi} \tag{29}$$

Mathematically Eqs. (27) -(29) lead to:

$$A_m = 0 \tag{30}$$

$$B_m = \frac{\left[\frac{Gt_w e k_{sh}}{a}\left(\frac{m\pi}{l}\right)\right]}{\left[EA_{tee}\left(\frac{m\pi}{l}\right)^2 + \frac{Gt_w k_{sh}}{a}\right]}C_m \tag{31}$$

$$C_m = \frac{1-(-1)^m}{(m\pi)^5}\frac{ql^4}{EI_{tee} + \dfrac{e^2 EA_{tee}}{1 + \dfrac{EA_{tee}\,a(m\pi)^2}{Gk_{sh}t_w l^2}}} \tag{32}$$

Therefore, the deflection of the castellated beam can be expressed as follows:

$$w(x) = \frac{ql^4}{E(I_{tee}+e^2 A_{tee})}\sum_{m=1,2,..}\frac{2}{(m\pi)^5}\left[1+\frac{e^2 A_{tee}}{I_{tee}+e^2 A_{tee}}\right.$$
$$\left. \times \frac{EA_{tee}\,a(m\pi)^2}{Gk_{sh}t_w l^2}\left(1-\frac{EI_{tee}\,a(m\pi)^2}{Gk_{sh}t_w l^2 e^2}\right)\right]\sin\frac{m\pi x}{l} \tag{33}$$

The maximum deflection of the simply supported beam is at the mid of the beam, that is *x=l/2* and thus it can be expressed as follows:

$$w|_{x=l/2} = \frac{ql^4}{E(I_{tee} + e^2 A_{tee})} \left[\sum_{k=1,2,..} \frac{2}{\pi^5} \frac{(-1)^{k+1}}{(2k-1)^5} + \frac{e^2 A_{tee}}{I_{tee} + e^2 A_{tee}} \times \frac{EA_{tee}\, a}{Gk_{sh} t_w l^2} \right.$$
$$\left. \times \left(\sum_{k=1,2,..} \frac{2}{\pi^2} \frac{(-1)^{k+1}}{(2k-1)^3} - \frac{EI_{tee}\, a}{Gk_{sh} t_w l^2 e^2} \sum_{k=1,2,..} \frac{2}{\pi} \frac{(-1)^{k+1}}{(2k-1)} \right) \right]$$

$$(34)$$

Note that, mathematically, the following equations hold,

$$\sum_{k=1,2,..} \frac{2}{\pi^5} \frac{(-1)^{k+1}}{(2k-1)^5} = \frac{5}{2 \times 384}$$

$$(35)$$

$$\sum_{k=1,2,..} \frac{2}{\pi^3} \frac{(-1)^{k+1}}{(2k-1)^3} = \frac{1}{16}$$

$$(36)$$

$$\sum_{k=1,2,..} \frac{2}{\pi} \frac{(-1)^{k+1}}{(2k-1)} = \frac{1}{2}$$

$$(37)$$

Using Eqs. (35), (36) and (37), the maximum deflection of the beam can be simplified as follows:

$$w|_{x=l/2} = \frac{5ql^4}{384E(2I_{tee} + 2e^2 A_{tee})} + \frac{ql^2 a}{16Gk_{sh} t_w} \times \left(\frac{eA_{tee}}{I_{tee} + e^2 A_{tee}} \right)^2$$
$$\times \left(1 - \frac{2EI_{tee}\, a}{Gk_{sh} t_w l^2 e^2} \right)$$

$$(38)$$

It is clear from Eq. (38) that, the first part of Eq. (38) represents the deflection generated by the bending load, which is deemed as that given by Bernoulli-Euler beam, while the second part of Eq. (38) provides the deflection generated by the shear force. Moreover, Eq. (38) shows that the shear-induced deflection is proportional to the cross-section area of the two T-sections but inversely proportional to the beam length. This explains why the shear effect could be ignored for long span beams.

If the calculation does not consider the shear effect of web openings, Eq. (38) reduces to the following bending deflection equation.

$$w|_{x=l/2} = \frac{5ql^4}{384EI_{reduced}}$$

$$(39)$$

Numerical Study

In order to validate the abovementioned analytical solution numerical analysis using the finite element method is also carried out. The numerical computation

11

uses the ANSYS Programming Design Language (APDL). The FEA modelling of the castellated beams is carried out by using 3D linear Quadratic 4-Node thin shell elements (SHELL181). This element presents four nodes with six DOF per node, i.e., translations and rotations on the X, Y, and Z axis, respectively. Half-length of the castellated beams is used because of the symmetry in geometry. The lateral and transverse deflections and rotation are restrained (u_y=0, u_z=0 and θ_x=0) at the simply supported end, while the symmetrical boundary condition is applied at the other end by constraining the axial displacement and rotations around the two axes within the cross-section (u_x=0, θ_y=0 and θ_z=0). The material properties of the castellated beam are assumed to be linear elastic material with Young's modulus E = 210 GPa and Poisson's ratio v =0.3.

A line load effect is used to model applied uniformly distribution load, where the load is assumed acting on the junction of the flange and the web. The equivalent nodal load is calculated by multiply the distribution load with beam's half-length and then divided by the number of the nodes on the junction line of the flange and the web.

Discussion

Figure 3 shows a comparison of the maximum deflations between analytical solutions using different shear rigidity factors including one with zero shear factor and FEA numerical solution for four castellated beams of different flange widths. It can be seen from the figure that, the analytical solution using the proposed shear factor is closest to the numerical solution, whereas the analytical solutions using other shear factors is not as good as the present one. This demonstrates that the shear factor is also affected by the ratio of the flange width to the beam length. Also, it can be seen from the figure that, the longer the beam, the closer the analytical solution to the numerical solution; and the wider the flanges, the closer the analytical solution to the numerical solution.

Figure 3. *Maximum Deflections of Simply Supported Castellated Beams with Uniformly Distributed Load Obtained using Analytical Solution with Different Shear Rigidity Factors (Eqs. (38) and (39)) and FEA Numerical Solution for Four Castellated Beams of Different Flange Widths (a) bf=100mm (b) bf=150mm (c) bf=200mm (d) bf=250mm (h_w=300mm, t_f=10mm, t_w=8mm and a=100mm)*
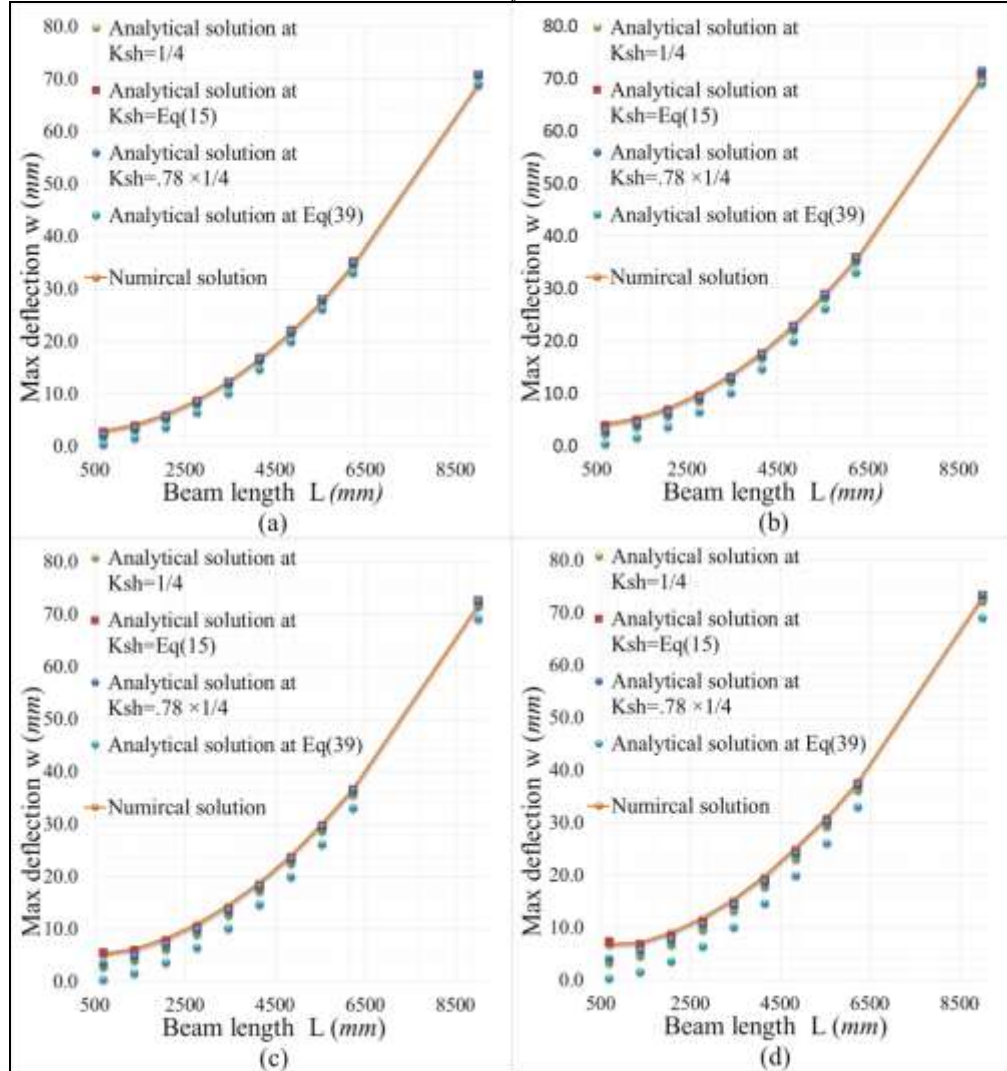
Figure 4 shows the relative error of each analytical solution when it is compared with the finite element solution. From the figure it is evident that the error of the analytical solutions using the present shear rigidity factor does not exceed 6.0% for all of discussed four sections in all the beam length range (>3 meter). In contrast, the analytical solution ignoring the shear effect, or considering the shear effect by using smear model or by using the length-independent shear rigidity factor will have large error, particularly when the beam is short.

Figure 4. *Divergence of Maximum Deflections of Simply Supported Castellated Beams with Uniformly Distributed Load Obtained using Analytical Solution with Different Shear Rigidity Factors (Eqs. (38) and (39)) and FEA Numerical Solution for Four Castellated Beams of Different Flange Widths* (a) *bf=100mm* (b) *bf=150mm* (c) *bf=200mm* (d) *bf=250mm* (h_w=300mm, t_f=10mm, t_w=8mm and a=100mm)
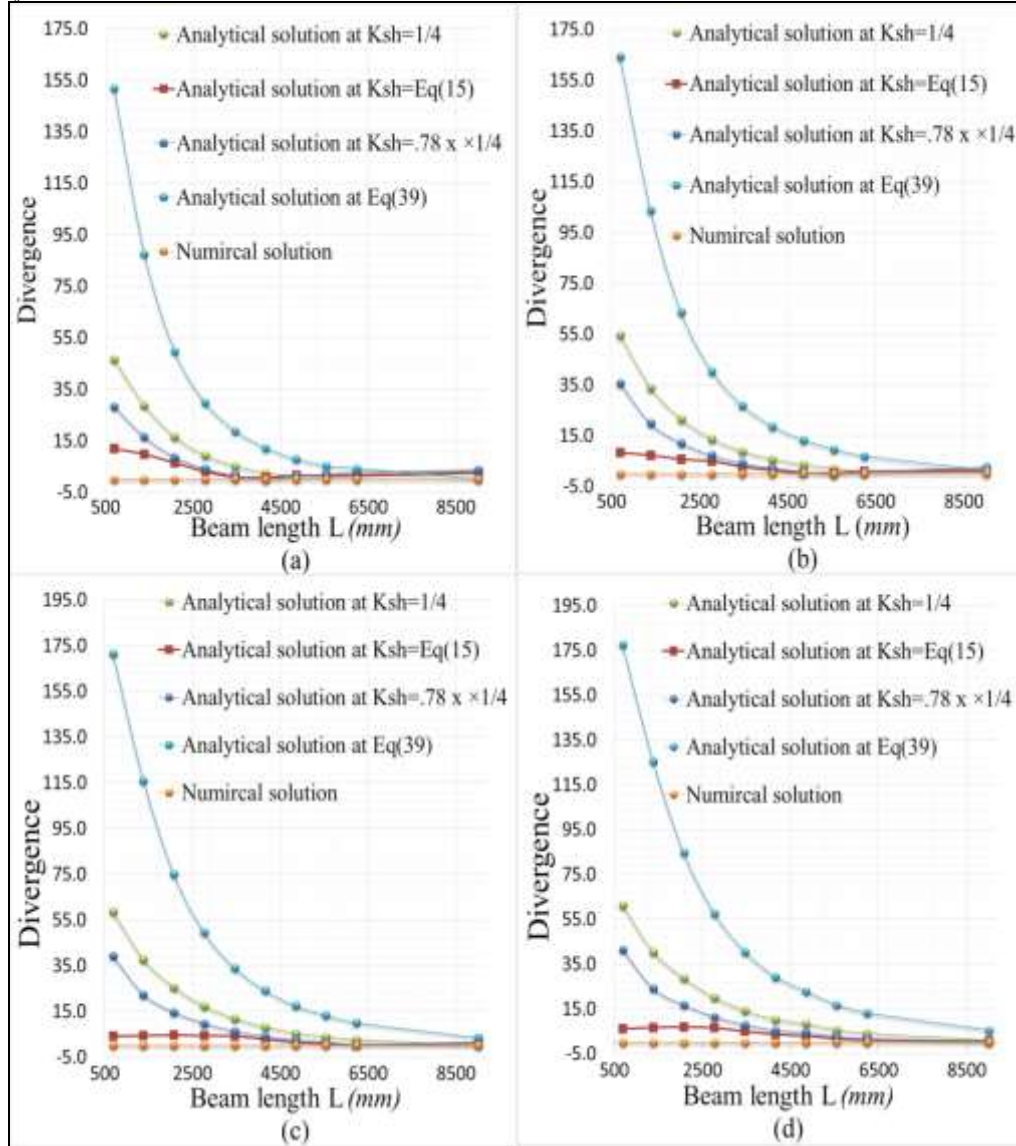
Conclusions

This study has reported the theoretical and numerical solutions for calculating the deflection of hexagonal castellated beams with simply supported boundary condition, subjected to a uniformly distributed transverse load. The analysis is based on the total potential energy method, by taking into account the influence of web shear deformations. The main novelty of the present analytical solution for

the calculation of deflection is it considers the shear effect of web openings more accurately. Both the analytical and numerical solutions are employed for a wide spectrum of geometric dimensions of I-shaped castellated beams in order to evaluate the analytical results. From the present study, the main conclusions can be summarized as follows:

1. The present analytical results are in excellent agreement with those obtained from the finite element analysis, which demonstrates the appropriateness of proposed approach.

2. Shear effect on the deflection of castellated beams is very important, particularly for short and medium length beams with narrow or wide section. Ignoring the shear effect could lead to an under-estimation of the deflection.

3. Divergence between analytical and numerical solutions does not exceed 6.0% even for short span castellated beam with narrow or wide section.

4. The effect of web shear on the deflection reduces when castellated beam length increases.

5. Despite that the numerical solution based on FEA has been widely used in the analysis of castellated beams; it is usually time-consuming and limited to specific geometrical dimensions. Thus, a simplified calculation solution that is able to deliver reasonable results but requires less computational effort would be helpful for both researchers and designers.

Acknowledgments

References

Altifillisch MD, Cooke RB, Toprac AA (1957) An Investigation of Open Web Expanded Beams. *Welding Research Council Bulletin, New York* 47: 307-320.

Aminian P, Niroomand H, Gandomi AH, Alavi AH, Arab Esmaeili M (2012) New Design Equations for Assessment of Load Carrying Capacity of Castellated Steel Beams: A Machine Learning Approach. *Neural Computing and Applications* 23(1): 119-131. http://doi:10.1007/s00521-012-1138-4.

Boyer JP (1964) Castellated Beam- A New Development Castellated Beams-New Developments. *AISC Engineering* 1(3): 104-108.

Demirdjian S (1999) *Stability of Castellated Beam Webs.* (PhD), McGill University Montreal, Canada.

Hosain M, Cheng W, Neis V (1974) Deflection Analysis of Expanded Open-Web Steel Beams. *Computers & Structures* 4(2): 327-336.

Kerdal D, Nethercot D (1984) Failure Modes for Castellated Beams. *Journal of Constructional Steel Research* 4(4): 295-315.

Kim B, Li L-Y, Edmonds A (2016) Analytical Solutions of Lateral–Torsional Buckling of Castellated Beams. *International Journal of Structural Stability and Dynamics*, 1550044. http://doi:10.1142/s0219455415500443.

Maalek S (2004) Shear Deflections of Tapered Timoshenko Beams. *International Journal of Mechanical Sciences* 46(5): 783-805. http://doi:10.1016/j.ijmecsci. 2004.05.003.

Sherbourne A, Van Oostrom J (1972) Plastic Analysis of Castellated Beams—Interaction of Moment, Shear and Axial Force. *Computers & Structures* 2(1): 79-109.

Soltani MR, Bouchaïr A, Mimoune M (2012) Nonlinear FE Analysis of the Ultimate Behavior of Steel Castellated Beams. *Journal of Constructional Steel Research* 70: 101-114. http://doi:10.1016/j.jcsr.2011.10.016.

Sonck D, Kinget L, Belis J (2015) *Deflections of Cellular and Castellated Beams.* Paper presented at the Future Visions (International Association for Shell and Spatial Structures) (IASS2015).

Srimani SS, Das P (1978) Finite Element Analysis of Castellated Beams. *Computers & Structures* 9(2): 169-174.

Wang P, Wang X, Ma N (2014) Vertical Shear Buckling Capacity of Web-Posts in Castellated Steel Beams with Fillet Corner Hexagonal Web Openings. *Engineering Structures* 75: 315-326. http://doi:10.1016/j.engstruct.2014.06.019.

Yuan W-B, Kim B, Li L-Y (2014) Buckling of Axially Loaded Castellated Steel Columns. *Journal of Constructional Steel Research* 92: 40-45. http://doi:10.1016/ j.jcsr.2013.10.013.

Yuan W-B, Yu N-T, Bao Z-S, Wu L-P (2016) Deflection of Castellated Beams Subjected to Uniformly Distributed Transverse Loading. *International Journal of Steel Structures* 16(3): 813-821.

Zaarour W, Redwood R (1996) Web Buckling in Thin Webbed Castellated Beams. *Journal of Structural Engineering* 122(8): 860-866.

Wheel Load Distribution in Four-Sided Concrete Box Culverts

By Elie Awwad[*]
Mounir Mabsout[†]
Kassim Tarhini[‡]
Hudson Jackson[♦]

This paper presents the results of a parametric study of wheel load distribution in four-sided precast concrete box culverts using three-dimensional finite element analysis (3D-FEA) as compared to the two-dimensional (2D) plane frame analysis. Maximum bending moments and deflections from the 3D-FEA results and the 2D frame analysis were computed and evaluated. Several concrete box culvert sizes were chosen with various span lengths, constant rise, and standard laying width. The culverts were subjected to various combinations of earth loading and AASHTO HS20 wheel loading applied at mid-span of the top slab. As the soil cover increases from 0 to 3 m, wheel loads are projected to the top slab using ASTM C890 procedure. The finite element results showed that the effect of wheel loading along mid-span is significant and that the edge loading condition for a single box is more critical than center loading for soil cover less than 0.9 m. The earth loading tends to gradually dominate as the soil cover increases, which is expected based on geotechnical engineering practices. It was shown that the plane frame analysis and 3D-FEA gave similar results for long-span and non-standard box culverts. However, for short-span (3.6 m) concrete box culverts, the plane frame analysis was less conservative than the 3D-FEA by about 15% for moments; versus about 5% for long-span culvert (7.2 m). The results of this paper will assist bridge engineers in analyzing and designing non-standard precast concrete box culverts and quickly replacing small bridges.

Keywords: *Concrete Box Culverts, Earth Pressure, Finite Element Analysis, Wheel Load Distribution.*

Introduction

According to the U.S.A. Federal Highway Administration's 2016 National Bridge Inventory data, 21.7% of the nation's 603,620 bridges are structurally deficient or functionally obsolete as reported in Better Roads Magazine (November 2016).[1] Highway Bridges that are either built using cast-in-place concrete or precast concrete panels form about 69% of all bridges (423,216). Single span reinforced concrete bridges represent about 150,000 and assuming 22% of those bridges to be structurally deficient or functionally obsolete. In the 2017 ASCE Infrastructure Report Card, ASCE cited almost 40% of all bridges are

[*]Associate Professor, Lebanese University, Lebanon.
[†]Professor, American University of Beirut, Lebanon.
[‡]Professor, U.S. Coast Guard Academy, USA.
[♦]Professor, U.S. Coast Guard Academy, USA.
[1]Better Roads Magazine (2016) *Annual Bridge Inventory* (Nov).

over fifty years or older and an additional 15% are between the ages of 40 and 49 years. The average bridge age in the U.S.A. was 43 years old while most of the bridges were designed for a lifespan of 50 years. Therefore, an increasing number of bridges will soon need major rehabilitation or replacement. However, this bridge inventory accounts for structures with span lengths greater than 6 m (20 ft), where the majority of the structurally deficient bridges are short spans, averaging less than 15 m (50 ft) in length. These deficient bridges are being recommended for weight-limit posting, rehabilitation, or decommissioning and replacement. Thousands of such structures especially with span length are less than 6 m (20 ft) in every state and municipality may be ignored, not inspected, or not replaced on regular basis due to the lack of funding. This task is left up to each local government to maintain structures spanning less than 6 m (20 ft) without federal support.

Cast-in-place reinforced concrete box culverts have been designed and used for many years because of special geometry or site conditions. As labor cost continues to rise, increase in traffic volume on highways, and the cost of inconvenience and delays associated with cast-in-place construction methods resulted in the introduction of precast concrete box culverts. To reduce cost and develop alternative to cast-is-place structures, prefabricated reinforced concrete culverts were developed as an economical alternatives for replacing deteriorating short-span bridges and cast-in-place culverts. These prefabricated structures include reinforced concrete arches, three- and four-sided concrete or metal box culverts. The most commonly used type is the precast reinforced concrete culvert due to its durability and minimal field construction time. There are two American Societies for Testing and Materials (ASTM) Specification for Precast Reinforced Concrete Box Culverts design standards: (i) ASTM C1433-16 (AASHTO M273) standard for culverts using AASHTO Standard Specifications, and (ii) ASTM C1577-16 (AASHTO M259) standard for culverts using AASHTO LRFD. Four-sided concrete culverts are typically referred to as box-culverts with standard span by rise sizes starting at 0.9 m X 0.6m (3 ft X 2 ft) and goes up to 3.6 m X 3.6 m (12 ft X 12 ft) with one-foot increment. The standard laying length is either 1.8 m or 2.4 m (6 ft or 8 ft) depending on the maximum weight limits generate per precast section and transport on the highway to the specific site. The maximum span length of a standard ASTM precast concrete box section is 3.6 m (12 ft) which may be too small to handle heavy water flow and may require the use of multiple sections placed side-by-side. In this case, the walls of adjacent culverts will act as a pier that may obstruct the flow of water and be associated with flooding problems. Therefore, developing new four-sided box sections with longer spans have proven to be an economical alternative to multiple box-sections.

This paper builds on the study reported by Awwad et al. (2008) by investigating the analysis of longer span 7.2 m (24 ft) culvert. The finite element analysis (FEA) results of four-sided reinforced concrete box culverts with span length of 7.2 m (24 ft) were compared to 2D frame analysis suggested by ASTM and AASHTO Standard Bridge Specifications (2002). The culvert had constant rise and was subjected to various load combinations of earth pressures and AASHTO HS20 wheel loading in the top slab. This study considered the effect of

each and/or combinations of soil cover on the culvert behavior, lateral earth pressures applied to side walls, and soil bearing pressure applied to the bottom slab. The results presented in this paper can assist bridge engineers in analyzing and designing precast concrete box culverts with span lengths longer than 3.6 m (12 ft) subject to various loads or load combinations of dead load, earth pressure, and live load.

Background

Precast concrete box culverts are typically designed as highway bridges per either AASHTO Standard (2002) or LRFD (2012). These specifications introduced the provision of distributing single or multiple wheel live loads to the bridge superstructure as a function of the depth of soil fill. Therefore, AASHTO suggest the analysis and design of box culverts by reducing the 3D structure to a 2D frame. Abolmaali and Garg (2008) reported the results of a study evaluating the shear behavior and capacity of 42 standard precast concrete box culverts presented in ASTM C1433 subject to AASHTO HS20 truck wheel load. No fill was placed on the top slab of the culverts and rigid bedding material was assumed to support the culverts. Full-scale experimental tests were conducted on 24 typical precast concrete box culverts designed as per ASTM C1433. Six full-scale 2.4 m span concrete box culverts were tested to failure by subjecting each culvert to the AASHTO HS20 wheel load. Each structure was loaded incrementally up to failure in which crack initiation and propagation were identified and recorded at each step. It was shown that all the test structures behaved in flexural mode up to and beyond the standard loads. Therefore, the test results indicated that flexure governed the behavior required by AASHTO Specifications. Three-dimensional nonlinear finite element models of the test structures were developed and compared with the experimental results. It was shown that the actual shear capacity exceeded the factored critical shear force for all the ASTM C1433 box culverts. The study concluded that shear is not the governing behavior mode for the concrete box culverts, and it was recommended that the live load distribution width equations along with the provisions for shear transfer devices for box culverts required in the AASHTO Standard must be revised. The study also concluded that there is no need for shear transfer device across the joints of adjacent precast concrete box culverts.

Awwad et al. (2008) reported the results of a study comparing the 3D-FEA versus 2D plane frame results of a new four-sided box culvert with span length of 5.4 m (18 ft) and a rise of 2.4 m (8 ft). The culvert was subjected to various combinations of earth loading from the soil cover, lateral earth pressure, and AASHTO HS20 wheel loading applied at center or edge along mid-span of the top slab. As the soil cover increases from 0 to 3 m (10 ft), wheel loads were projected to the top slab using ASTM C890 procedure. The results showed that the effect of wheel loading along mid-span is significant and that the edge loading condition for a single box is more critical than center loading for soil cover less than 0.9 m (3 ft). The earth fill loading tends to gradually dominate as the soil cover increases. It

was shown that moments from plane frame analysis and 3D FEA gave similar results.

Orton et al. (2015) reported experimental data from field testing of multi-cell reinforced concrete box culverts under soil fill. This study was performed to quantify the reduction of live-load effects with increasing fill depth since the current structural analysis procedures are overly conservative in predicting the live-load effects. The study investigated experimentally the effects of truck loads on reinforced concrete box culverts classified as bridges (where spans are greater than 6 m (20 ft)) under soil fills of different thickness. The study considered ten existing reinforced concrete box culverts with fill depths ranging from 0.76 m (2.5 ft) to 4.1 m (13.5 ft). Test results showed that the live-load effect does diminish with increasing fill depth. It was shown that at depths beyond 1.82 m (6 ft), the live-load pressures are less than 10% of the dead-load pressure, and this fill depth was considered as a point at which live-load effects may be neglected. This conclusion matches the results reported earlier by Awwad et al. (2008). Furthermore, the AASHTO LRFD Bridge Design Specifications (2012) were found to be overly conservative in predicting strains and displacements compared with field data for fill depths less than 2.4 m (8 ft). The primary source of conservatism is likely the two-way action in the top slab of the culvert.

Acharya et al. (2016) reported the results of a parametric study by investigating the influence of concrete pavement thickness, fill depth, wheel loads, and culvert span on the load distributions. The study was based on the results of a comprehensive field study of a single-cell low-fill box culvert. The culverts were instrumented with displacement transducers and pressure cells to capture deformations and pressures resulting from different combinations of wheel loads. It was shown that the intensity of the vertical pressure gradually decreased with an increase in the concrete pavement thickness and fill depth because the wheel load was distributed over a wider area. The vertical pressure on top of the culvert decreased with the increase of the culvert span. The study demonstrated that the AASHTO pressure distribution methods are overly conservative for the wheel load distribution on a low-fill box culvert under rigid pavement. The difference in the calculated vertical pressure decreased with the increase of the fill depth. For all the fill depths considered, the calculated pressure by the AASHTO LRFD code was higher than that by the AASHTO Standard Specifications. At the higher fill depth (2.4 m) and wider span, the calculated pressure by the AASHTO Standard Specification closely matched the pressure found by the numerical method.

Description of Box Culverts

Geometry

A typical three-dimensional precast concrete box culvert is shown in Figure 1. The main geometric parameters of a box culvert are the span length, rise, laying width, haunches, wall thickness and top/bottom slab thicknesses. A box culvert with span length (S) of 7.2 m (24 ft) is investigated in this study. The culvert had

constant rise of 2.4 m (8 ft), constant slab and wall thicknesses of 0.3 m (1 ft), and haunches at each corner of 0.3 m x 0.3 m (1 ft x 1 ft). The laying width of the section was chosen as the standard 1.8 m (6 ft). The box section selected for this study was labeled as B24, which correspond to the span length. The overall weight and possible transporting the box culvert to a construction site was not addressed in this investigation.

It should be noted that this longer culvert of 7.2 m (24 ft) was selected to fill a need to provide practical structural analysis of concrete box culverts spanning more than 3.6 m (12 ft) and less than 9 m (30 ft). The ASTM Standard covers precast culverts with spans up to 3.6 m (12 ft), and this research will allow engineers to address box culverts reaching up to 7.2 m (24 ft).

Figure 1. *Typical 3D Precast Concrete Box Culvert*
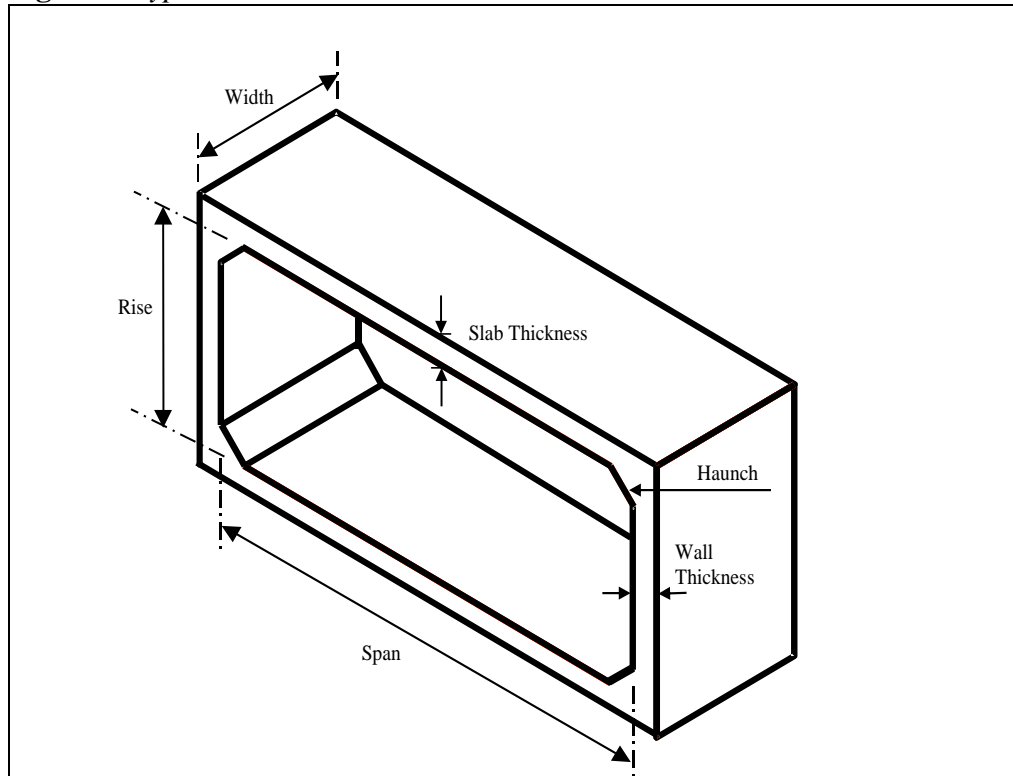
Material Properties

The material properties used in modeling the precast concrete box culvert was assumed to be normal-strength concrete with compressive strength of 27.6 MPa (4,000 psi), modulus of elasticity 24.8 GPa (3.6×10^6 psi), and Poisson's ratio 0.2. A typical 19 kN/m^3 (120 lbs/ft^3) unit weight "γ" of soil was used and a friction angle ϕ was assumed to be 30° for well-drained granular fill material. The soil is considered at rest condition with a lateral pressure coefficient k_0 of 0.5 (where $k_0 = 1 - sin\phi$). To be conservative, it was assumed that the depth of water table to be below the culvert and there was no stream running water.

Loading

Figure 2 shows the various critical applied loads that will influence the load distribution in precast concrete box culverts. The culverts were subjected to overburden pressure due to soil cover, lateral earth pressures, and the standard AASHTO HS20 truck wheel load. The culvert self-weight was included in the comparative analysis of 3D-FEA vs 2D frame analysis. However, the culvert self-weight should be part of the load combination of the soil and live loadings in the final analysis and design of the culverts. The height of soil cover *(Z)* above the top slab was varied from 0 m (no cover) to 3 m (10 ft), with increments of 0.6 m (2 ft) and the resulting overburden pressure *(γZ)* was applied uniformly to the top slab. The lateral earth effect was modeled as linearly varying trapezoidal pressures on the culverts walls, starting with $(k_0 \gamma Z)$ at the top slab level. The soil bearing pressure below the bottom slab was modeled by means of linear springs of 268 kN/m^2/m (50 lbs/in^2/in).

Figure 2. *Typical Earth and HS20 Wheel Loading on the Culvert*
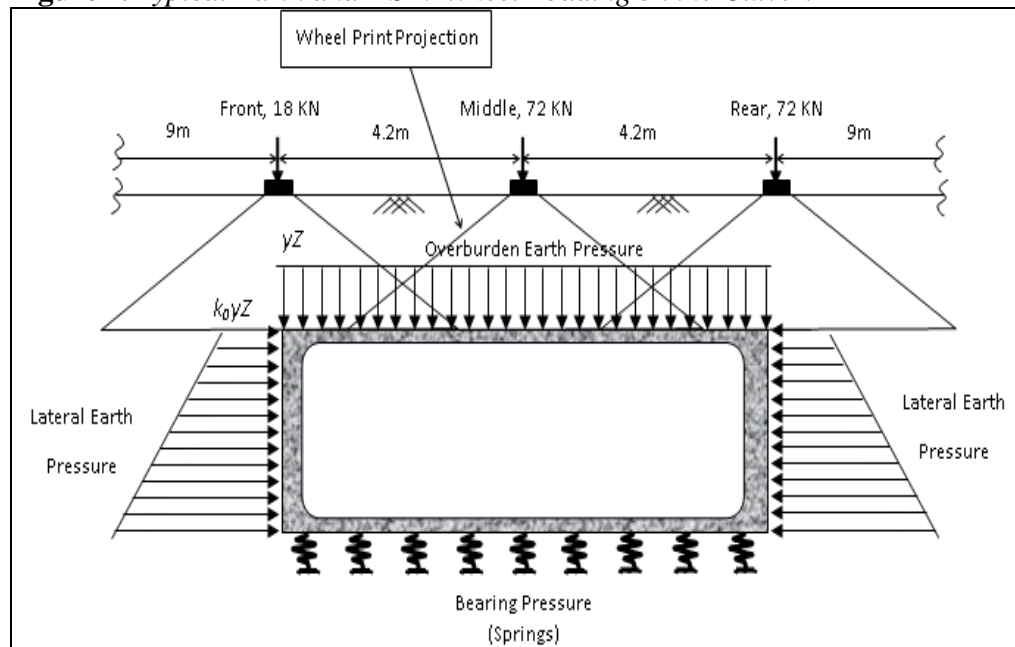
In the 3D-FEA, AASHTO HS20 truck consists of 2 lines of wheels spaced 1.8 m (6 ft) apart. Each line has 18, 72, and 72 kN (4, 16, and 16 kips) concentrated wheel loads as shown in Figure 2. AASHTO and ASTM C1433 (2016) specify that a wheel load is to be applied as a tire print over an area of 0.50 m x 0.25 m (20 in x 10 in) directly to the top slab of a culvert for soil cover less than or equal to 0.6 m (2 ft). For soil cover more than 0.6 m (2 ft), the tire print area is projected using ASTM C890 (2013) equation *(W + 1.75Z)* x *(L + 1.75Z)*, where *W* is the width (20 in) and *L* is the length (10 in) of the tire print. Two wheel loading positions along mid-span are considered: (i) Centered Loading where the projection of the tire print of the middle wheel is placed in the center of top slab along mid-span and (ii) Edge Loading where the projection of the tire print of the

wheel is placed at the edge of top slab along mid-span. These two loading conditions were considered based on a study by Awwad et al. (2008) in which several wheel load positions were investigated, located from edge to center along mid-span. The maximum values of bending moments and deflections in the top slab, as expected, decreased as the tire print was moved from edge toward the center. The centered and edge wheel loadings along mid-span were therefore selected to represent extreme loading conditions encompassing all other possible intermediate wheel load positions. The AASHTO Standard Bridge Specifications (2002) consider an impact factor for the dynamic live load effect as follows: 30% increase in wheel load for soil cover less than 0.3 m (1 ft), 20% increase in wheel loads for soil cover between 0.3 and 0.6 m (1 and 2 ft), 10% increase in wheel loads for soil cover between 0.6 and 0.9 m (2 and 3 ft), and no impact for soil covers more than 1.2 m (4 ft).

Load Combinations

The concrete box culvert selected for this study was analyzed, subject to the variable soil pressure and static wheel loading described earlier. The culvert was subjected to both Centered and Edge wheel loadings. In addition, soil loading was applied in three stages as follows: Case 1 considers only the overburden pressure on the top slab for the various soil covers selected and assumes the culverts to be simply supported by hinges under the side walls. Case 2 is similar to Case 1 but with the addition of lateral earth pressure applied to the side walls. Case 3 considers all soil pressures on the culvert slabs and walls, in addition to bearing springs under the bottom slab which support the culverts. The concrete culvert was analyzed considering the various load combinations of six soil covers, two wheel positions, and three earth loading cases.

Finite Element Modeling

The concrete box culverts were modeled using the finite element analysis computer program SAP2000.[2] A mesh sensitivity analysis was conducted and a suitable discretization using 0.15 m x 0.15 m (0.5 ft x 0.5 ft) four-node shell elements with six degrees of freedom at each node was adopted. The concrete slabs and walls were modeled as linear elastic four-node shell elements that account for plate bending in the slab, and bending with axial behavior in the side walls. The shell thickness of 0.3 m (12 in) was used for the slabs and walls while haunches are modeled using an equivalent thickness of 0.38 m (15 in).

The concrete box culverts were also analyzed as 2D plane frames per ASTM and AASHTO procedures. A unit-width is considered in the analysis and the corresponding earth pressures are applied in the three stages discussed earlier. For soil cover less than or equal to 0.6 m (2 ft), the middle tire print of the HS20 truck is applied at mid-span of the top frame member and is divided by the distribution

---

[2]SAP2000 (Version 17) Berkeley, California: Computers and Structures Inc.

width suggested by AASHTO Standard Bridge Specifications (2002), E (ft) = $4 + 0.06S_{eff}$, where S_{eff} (ft) is the effective span length, measured between mid-haunches (S_{eff} = clear span S – haunch width). When the soil cover exceeds 0.6 m (2 ft), the tire prints are projected using procedures specified in ASTM C890. Noting that the centered and edge wheel loading condition become identical in the 2D analysis.

The finite element model of a typical culvert B24 subjected to edge wheel loading, overburden and lateral earth pressures with Z = 0.6 m (2 ft), supported by bearing springs distributed below the bottom slab, as described in Case 3. The corresponding deflected box culvert and longitudinal bending moment distribution in the slabs and walls are shown in Figure 3. The longitudinal moment is the bending moment about the transverse axis which is used in determining the main reinforcing steel in the culvert.

Figure 3. *Deflection and Bending Moment in Culvert B24 under Edge Loading (Case 3, Z = 0.6 m)*
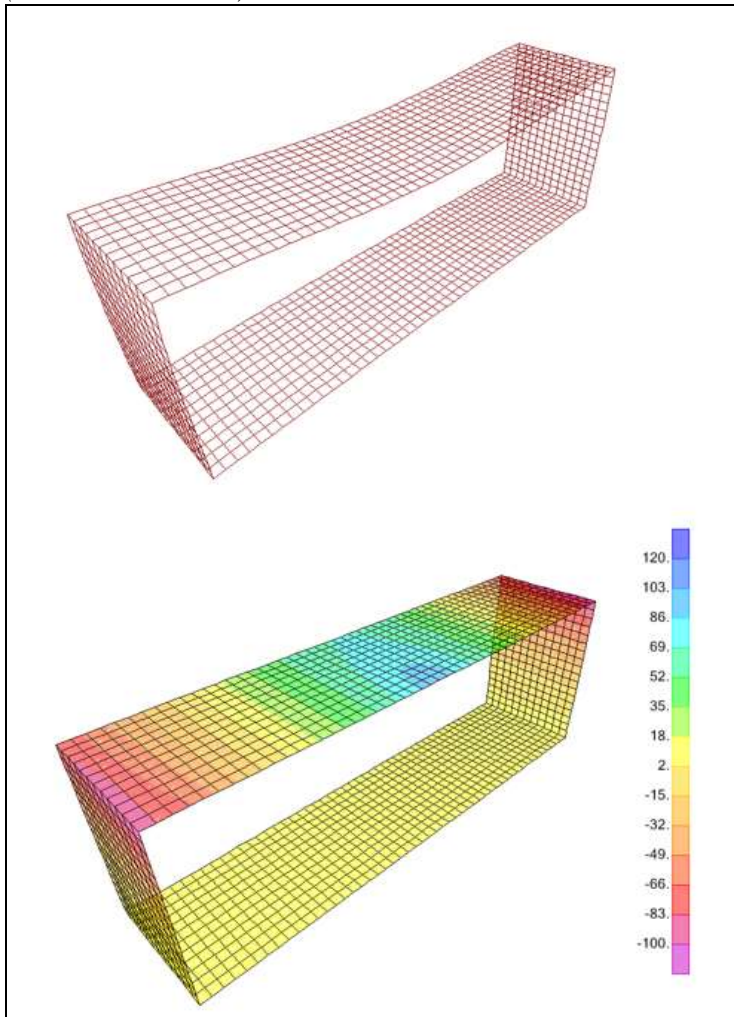
Results

The critical bending moments (M_p and M_n) were identified at mid-span and the wall support of the top slab along with the maximum vertical deflection (D) at mid-span for all culverts and load cases considered in this investigation. The maximum positive bending moments, negative bending moments, and deflections for all three culverts (B12, B18, and B24) investigated by Awwad (2008) are summarized in Table 1. Typical FEA results for the culvert with span length of 7.2 m (24 ft or B24) for Case 1 are shown in Figure 4. The 3D FEA and 2D Frame analysis results are plotted along the culverts laying width (1.8 m or 6 ft) for selected soil covers (Z = 0.6 m (2 ft) and 1.8 m (6 ft)) for individual edge and centered tire loading, earth loading, and total combined tire and earth loading.

General observations can be made to all three culverts (B12, B18, and B24) results that were summarized in Table 1. The edge condition results are higher than the centered ones for soil covers "Z" less than 0.6 m (2 ft). The difference between edge and centered conditions decreases when the soil cover exceeds 1.2 m (4 ft), and becomes insignificant for soil cover greater than 3 m (10 ft). This is consistent with geotechnical engineering practice, the deeper soil cover tends to lessen the influence of the wheel load position and its concentration by spreading it more evenly to the top slab. The effect of overburden pressure only (Case 1), overburden and lateral earth pressure (Case 2), and overburden, lateral, and bearing pressure (Case 3) on the box culvert were analyzed and compared with reference Case 1. The lateral pressure added in Case 2 tends to camber the top slab upwards, resulting in a decrease in the positive moments and deflections and an increase in the negative moments in the top slab. Applying bearing pressure to the bottom slab in Case 3 has the reverse counter effect. The results in Table 1 showed that the difference between the three load cases is more significant for the short-span culvert B12, and is less significant for the long-span culverts B18 and B24, namely between Case 1 and Case 2. This is due to the fact that the lateral pressure effect in Case 2 is similar for all three spans considered since the culvert rise is kept constant; the lateral effect will therefore be more significant for the short-span culverts with relatively smaller values of moments and deflections in the top slab.

The FEA results for culvert B12 showed a decrease of approximately 13% in the maximum positive moment in the top slab for the load case with lateral pressure (Case 2 versus Case 1); this decrease is reduced to about 4% when bearing pressure was added (Case 3 versus Case 1). Correspondingly, an increase in the maximum negative moments of about 15% and 4% is observed when considering Cases 2 and 3 versus Case 1, respectively. The maximum deflection in the top slab is also decreased by about 20% for Case 2, compared to Case 1. The deflection resulted from load Case 3 is excluded from the comparison since it includes the settlement due to presence of bearing springs.

Table 1. *Box Culverts B12, B18, and B24: Maximum Positive Moments, Negative Moments, and Deflections for All Cases and Conditions Considered*

Culvert B12 Maximum Values		Z = 0 m			Z = 0.6 m			Z =1.2 m			Z = 1.8 m			Z = 2.4 m			Z = 3.0 m		
		Case 1	Case 2	Case 3	Case 1	Case 2	Case 3	Case 1	Case 2	Case 3	Case 1	Case 2	Case 3	Case 1	Case 2	Case 3	Case 1	Case 2	Case 3
M positive (kN-m/m)	FEA-3D-Center	33.84	30.69	32.45	42.57	37.98	41.13	35.15	28.94	33.26	43.16	35.46	41.22	51.71	42.53	49.59	62.69	51.93	60.53
	FEA-3D-Edge	49.19	46.04	47.79	56.93	52.29	55.49	37.31	31.10	35.60	45.05	37.49	43.47	52.74	43.52	50.72	62.69	51.93	60.53
	2D-Frame	40.68	37.53	39.69	49.05	44.37	47.88	34.70	28.53	32.63	41.76	34.07	39.51	50.63	41.40	48.15	60.30	49.55	57.56
M negative (kN-m/m)	FEA-3D-Center	19.76	22.82	21.11	29.84	34.43	31.28	34.20	40.28	36.00	43.20	50.76	45.09	51.98	61.02	54.00	63.00	73.49	65.03
	FEA-3D-Edge	29.07	32.22	29.97	37.94	42.66	39.02	36.18	42.26	37.80	45.23	52.79	46.85	53.01	62.01	54.86	63.00	73.49	65.03
	2D-Frame	24.57	27.72	25.56	34.02	38.70	35.19	33.21	39.38	35.28	41.27	48.96	43.52	50.13	59.31	52.61	59.67	70.38	62.42
Deflection (mm)	FEA-3D-Center	0.44	0.35	0.70	0.64	0.51	1.15	0.71	0.53	1.38	0.88	0.66	1.81	1.06	0.79	2.21	1.28	0.97	2.70
	FEA-3D-Edge	0.65	0.56	1.37	0.84	0.70	1.78	0.75	0.57	1.47	0.92	0.70	1.91	1.08	0.81	2.27	1.28	0.97	2.70
	2D-Frame	0.60	0.51	0.97	0.79	0.66	1.41	0.72	0.54	1.40	0.88	0.66	1.79	1.07	0.80	2.21	1.27	0.96	2.65

Culvert B18 Maximum Values		Z = 0 m			Z = 0.6 m			Z =1.2 m			Z = 1.8 m			Z = 2.4 m			Z = 3.0 m		
		Case 1	Case 2	Case 3	Case 1	Case 2	Case 3	Case 1	Case 2	Case 3	Case 1	Case 2	Case 3	Case 1	Case 2	Case 3	Case 1	Case 2	Case 3
M positive (kN-m/m)	FEA-3D-Center	45.90	43.47	44.87	64.49	60.89	63.99	64.17	59.45	64.04	81.90	76.01	82.40	99.86	92.84	100.98	122.27	114.08	124.07
	FEA-3D-Edge	61.65	59.22	60.66	79.25	75.69	78.80	67.68	62.96	67.68	85.46	79.56	86.13	101.75	94.73	103.05	122.27	114.08	124.07
	2D-Frame	52.34	49.91	51.48	70.56	66.96	70.20	63.63	58.86	63.32	79.88	73.94	80.06	96.35	89.28	96.98	117.18	108.95	118.26
M negative (kN-m/m)	FEA-3D-Center	31.41	33.75	32.36	56.43	59.85	56.84	73.85	78.39	73.94	98.28	103.91	97.83	122.36	129.02	121.14	149.81	157.64	147.96
	FEA-3D-Edge	39.20	41.72	39.74	61.61	65.34	61.65	77.31	81.81	77.27	102.15	107.78	101.57	124.61	131.36	123.30	149.81	157.64	147.96
	2D-Frame	36.18	38.61	36.99	59.85	63.41	60.21	70.88	75.60	71.19	93.20	99.09	93.06	114.35	121.41	113.72	139.05	147.29	137.97
Deflection (mm)	FEA-3D-Center	1.20	1.05	1.50	2.01	1.79	2.81	2.52	2.22	3.70	3.30	2.93	5.03	4.05	3.63	6.30	4.98	4.45	7.75
	FEA-3D-Edge	1.55	1.40	2.21	2.34	2.11	3.48	2.65	2.35	3.90	3.43	3.08	5.23	4.13	3.70	6.43	4.98	4.45	7.75
	2D-Frame	1.49	1.34	1.88	2.29	2.07	3.18	2.55	2.25	3.73	3.28	2.93	4.98	4.00	3.55	6.15	4.85	4.35	7.50

Culvert B24 Maximum Values		Z = 0 m			Z = 0.6 m			Z =1.2 m			Z = 1.8 m			Z = 2.4 m			Z = 3.0 m		
		Case 1	Case 2	Case 3	Case 1	Case 2	Case 3	Case 1	Case 2	Case 3	Case 1	Case 2	Case 3	Case 1	Case 2	Case 3	Case 1	Case 2	Case 3
M positive (kN-m/m)	FEA-3D-Center	57.78	55.85	56.79	89.55	86.63	89.15	100.26	96.44	100.62	131.49	126.77	132.48	161.37	155.66	162.90	197.24	190.62	199.44
	FEA-3D-Edge	73.71	71.73	72.68	104.49	101.57	104.09	105.21	101.39	105.66	136.85	132.08	137.97	164.16	158.45	165.83	197.24	190.62	199.44
	2D-Frame	62.33	60.35	61.38	93.92	90.99	93.51	99.68	95.85	99.90	128.84	124.07	129.60	157.46	151.70	158.63	191.43	184.77	193.19
M negative (kN-m/m)	FEA-3D-Center	43.56	45.36	44.46	90.32	92.97	90.63	129.11	132.62	129.20	176.99	181.40	176.49	221.63	226.89	220.05	270.90	277.02	268.74
	FEA-3D-Edge	49.41	51.53	50.00	94.23	97.07	91.13	134.33	137.88	134.42	183.42	187.83	182.93	225.45	230.72	223.79	270.90	277.02	268.74
	2D-Frame	46.53	48.51	47.48	90.90	93.78	91.26	123.35	127.22	123.57	166.95	171.72	166.64	207.36	213.08	206.15	252.18	258.84	250.43
Deflection (mm)	FEA-3D-Center	2.52	2.31	2.82	4.78	4.48	5.83	6.50	6.08	8.30	8.75	8.23	11.30	10.88	10.25	14.18	13.28	12.58	17.38
	FEA-3D-Edge	3.00	2.80	3.63	5.23	4.93	6.58	6.78	6.35	8.68	9.08	8.55	11.75	11.05	10.45	14.43	13.28	12.58	17.38
	2D-Frame	2.90	2.68	3.25	5.15	4.85	6.25	6.55	6.13	8.35	8.70	8.20	11.23	10.75	10.15	13.98	13.08	12.38	17.03

Figure 4. (a) *Positive Moment* (b) *Negative Moment* and (c) *Deflections Results under Wheel Loading (Center and Edge) and Earth Pressure (Case 1, Z= 0.6 m and 1.8 m) for Culvert B24*
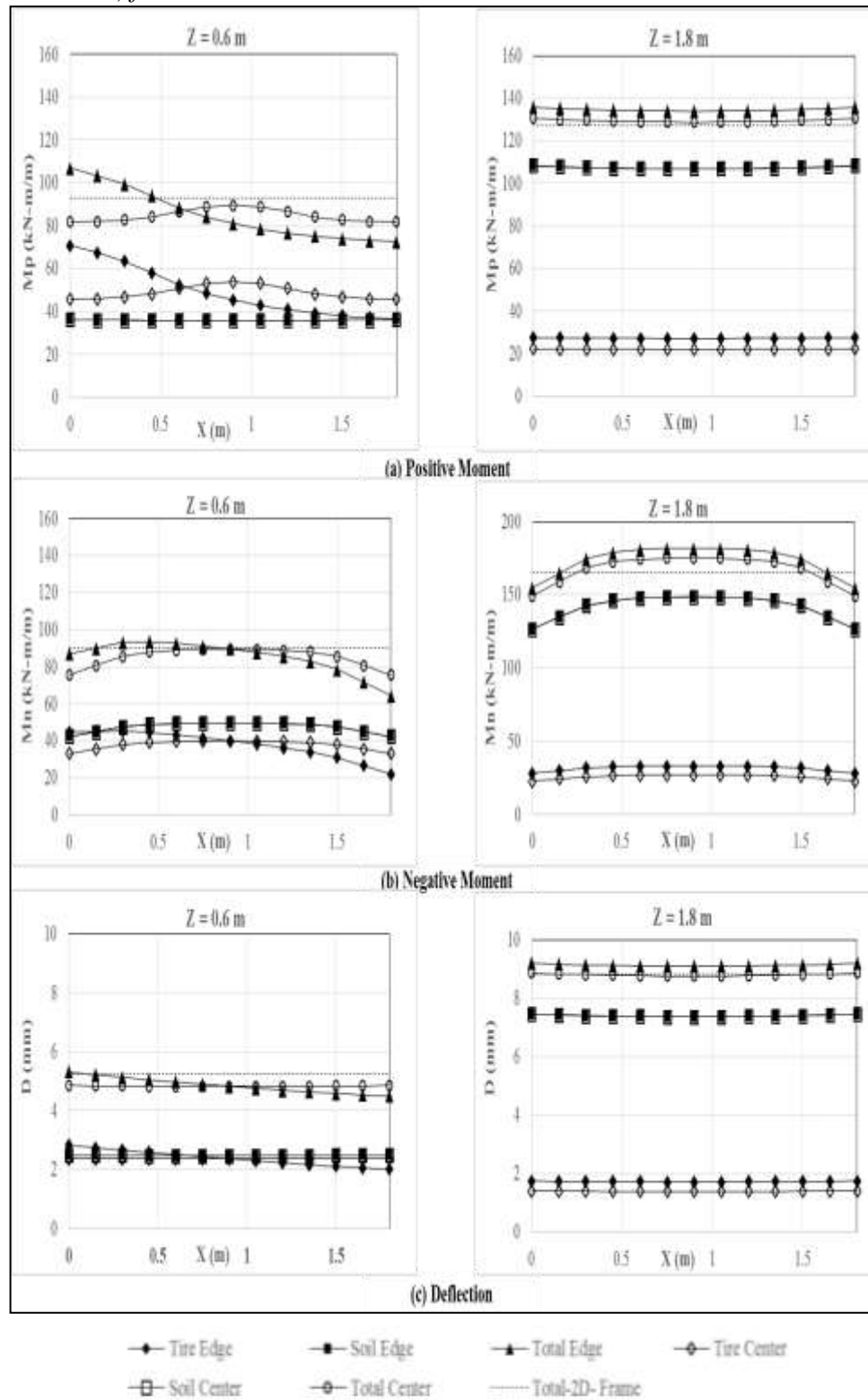
For the other two culverts B18 and B24, the finite element results indicated that an average of 5% increase is observed in the maximum positive or negative moments when lateral pressure is included (Case 2 versus Case 1) and almost no changes occur when bearing pressure is added (Case 3 versus Case 1). A decrease of 8% in the maximum deflection is observed for loading Case 2 versus Case 1. It was also noted that the percent increase or decrease in moments and deflections with respect to Case 1 are similar for 3D-FEA, center and edge, and 2D plane frame analyses.

The 3D-FEA results were compared with 2D plane frame analysis recommended by AASHTO Bridge Specifications and ASTM standards. The average bending moments and deflections were obtained for the three load Cases 1, 2, and 3. For soil cover less than 0.9 m (3 ft) and centered tire loading condition, 2D plane frame analysis overestimates the maximum positive and negative moments by 15%, 10%, and 5% for culverts B12, B18, and B24 respectively; the maximum deflections were overestimated by 25%, 17%, and 10%, for Culverts B12, B18, and B24, respectively. For soil cover less than 0.9 m (3 ft) and edge wheel loading condition, the 2D frame analysis underestimates the maximum positive and negative moments by about 17%, for Culvert B12, and by about 10% for Culverts B18 and B24. However, the maximum deflections was about 3% difference for all three culverts. For soil cover more than 0.9 m (3 ft), the results for centered and edge tire loading conditions were similar to the 3D-FEA and slightly greater than the 2D plane frame for all three culverts, reaching about 5% increase for edge loading.

Conclusions

This paper presented the results of a parametric study investigating the structural response of four-sided concrete box culverts using finite element analysis. Three culverts span lengths (B12, B18, and B24) were selected and analyzed under various load combinations of wheel load, earth pressure, and various soil covers. For soil fill up to 0.9 m (3 ft), it was observed that the wheel loading is dominant and it was found that the edge wheel loading was more critical than centered wheel loading at mid-span. As the soil cover increases above 0.9 m (3 ft), it was expected that the earth loading tends to gradually dominate, and for soil cover exceeding 2.1 m (7 ft), the live wheel loading effect was found to be negligible when compared to dead load due to earth fill loading. Load cases with lateral earth pressure applied to side walls (Case 2) and bearing pressure applied to the bottom slab in addition to lateral pressure (Case 3), were compared with the case when only overburden pressure is applied to the top slab (Case 1). It was observed when comparing Case 2 loading combination relative to Case 1 loading: (a) the positive moments decreased by 13% for B12 and increased by 5% for B18 and B24; (b) the negative moments increased by 15% for B12 and increased by 5% for B18 and B24; and (c) the deflections decreased by 20% for B12 and decreased by 8% for B18 and B24. It was concluded that plane frame analysis leads to slightly conservative bending moment results when compared to 3D-FEA,

it was off by 15% for short-span culverts (B12), 10% for B18, and 5% for longer span (B24) culverts.

References

AASHTO (2002) *Standard Specifications for Highway Bridges*, 17th Edition. Washington, D.C.: American Association of State Highway and Transportation Officials (AASHTO).

AASHTO (2012) *LRFD Bridge Design Specifications*. 7th Edition. Washington, D.C.: American Association of State Highway and Transportation Officials (AASHTO).

Abolmaali A, Garg A (2008) Shear Behavior and Mode of Failure for ASTM C1433 Precast Box Culverts. *Journal of Bridge Engineering* 13(4): 331-338.

Acharya R, Han J, Parsons R (2016) Numerical Analysis of Low-Fill Box Culvert under Rigid Pavement Subjected to Static Traffic Loading. *International Journal of Geomechanics* 16(5) 04016016.

ASTM - American Society for Testing and Materials (2013) *Standard Practice for Minimum Structural Design Loading for Monolithic or Sectional Precast Concrete Water and Wastewater Structures*. West Conshohocken, PA: C890-13, ASTM International.

ASTM - American Society for Testing and Materials (2016) *Standard Specification for Precast Reinforced Concrete Monolithic Box Sections for Culverts, Storm Drains, and Sewers*. West Conshohocken, PA: C1433-16, ASTM International.

ASTM - American Society for Testing and Materials (2016) *Standard Specification for Precast Reinforced Concrete Monolithic Box Sections for Culverts, Storm Drains, and Sewers Designed according to AASHTO LRFD*. West Conshohocken, PA: C1577-16, ASTM International.

Awwad E, Mabsout M, Sadek S, Tarhini K (2008) Parametric Study of Load Distribution in Four-Sided Concrete Box Culverts. *Journal of Bridge Structures* 4(2): 99-107.

Orton S, Loehr JE, Boeckmann A, Havens G (2015) Live-load Effect in Reinforced Concrete Box Culverts under Soil Fill. *Journal of Bridge Engineering* 20(11) 04015003.

Parametric Study for Performance of R.C. Wall with Opening using Analytical F.E. Model

By Alaa Morsy[*] & Youssef Ibrahim[†]

Earthquake is a catastrophic event, which makes enormous harm to properties and human lives. R.C. walls are provided in structures to decrease horizontal displacements under seismic load. R.C walls in residential buildings might have openings that are required for windows, doors or different states of openings due to architectural purposes. Size, position, and area of openings may fluctuate from an engineering perspective and might have an impact on stiffness of R.C wall and on the structures seismic reaction. F.E. modeling approach has been conducted to study effects of opening shape, size and position in RC wall with different thicknesses under axial & lateral static loads. F.E. Method using "ANSYS" becomes an essential approach in analyzing civil engineering problems numerically. Now we can make various models with different parameters in short time by using ANSYS instead of examining it experimentally, which consumes much time and money. The proposed F.E approach has been verified with experimental programs conducted by other researchers and gives a perfect correlation between the model and experimental outputs including load capacity, failure mode, crack pattern and lateral displacement. A parametric study is applied to investigate effects of opening size, shape, orientation, aspect ratio, position with different R.C. wall thicknesses. After verifying the proposed F.E approach with other mathematical design models conducted by other researchers, a statistical analysis was performed on 38 F.E. specimens and is presented in this paper. Outcomes of this statistical analysis provide an overview of the performance of current design models and identify research gaps. The findings presented herein will be used to define a new mathematical formula to provide the ultimate axial load of R.C. wall with circular opening. This research may be useful for improving existing design models and to be applied in practice, as it satisfies both architectural and structural requirements.

Keywords: *ANSYS, F.E.M., Opening, Seismic, Shear Wall.*

Introduction

Shear walls are vertical structural elements designed to resist lateral forces exerted on a building by the lateral loads that may be induced by the effect of wind and earthquakes. But shear walls are frequently pierced for doors, windows and building services or other functional reasons. Openings are usually avoided in reinforced concrete structural elements because the size and location of openings in the shear wall may have adverse effect on seismic responses. These openings are also source of weak points and cause decrease inside the structure's stiffness and load-bearing capacity. As a designer, it is

---

[*]Associate Professor, The Arab Academy for Science, Technology & Maritime Transport, Egypt.
[†]Post Graduate Student, The Arab Academy for Science, Technology & Maritime Transport, Egypt.

important to know the impacts of large openings sizes and configurations in shear wall on stiffness and also on seismic responses and behavior of structural system as a much amount of concrete and reinforcing steels has to be removed. So, an optimum configuration of openings in shear walls needs to be made (Lin and Kuo 1988).

Behavior of shear wall with openings has been studied in number of researches. Lin and Kuo (1988) conducted finite element analysis and experimental work to examine the ultimate strength of shear wall with openings under the effect of lateral load. The test program demonstrated the shear behavior of R.C. walls with different sizes of openings and reinforcing patterns around the opening. It was resolved that the shear capacity of the section is not only affected by the width of openings but also affected by the depth of openings as well which is not included in ACI Code.

Chowdhury et al. (2012) has modeled a six-storey frame-shear wall building using ETABS and studied the effects of openings in core type shear wall of thickness 203 mm under earthquake loads in equal static analysis. The results found out that stiffness and seismic response of the structure is affected by the dimensions of openings and position of openings in shear walls. It is also concluded that the more size of opening the more displacements conceded via building and this trend will increase with increasing storey level. Increasing wall thickness around the door openings are extra effective than that of window opening as far as displacement is concerned at top most story level. Furthermore, it is clearly definitely that opening in shear wall positioned in plane of loading is extra critical than that of opening in shear wall located out of plane of loading due to the fact that there is a significant change in displacement noticed after having opening in shear wall positioned in plane of loading.

Mosoarca (2014) analyzed the seismic behavior of shear walls with regular and staggered openings after the strong earthquake. He modeled a three-storey shear wall of thickness 120 mm on a scale of 1/3 and statically loaded them with alternating cyclic horizontal loads. The study concluded that, with the same amount of reinforcement and layout, the walls with staggered openings developed a ductile failure, whereas the ones with regular openings developed a brittle failure; and the shear walls with staggered openings are more rigid and needed less reinforcement. Therefore, the opening location affects the shear wall capacity.

Musmar (2013) has modeled a five-storey frame-shear wall building using ANSYS and studied the effects of openings size in shear wall of thickness 300 mm. The openings are placed in all stories at the mid length of shear walls. Adopted openings length is 1m, and the opening height is variable starting from 0.5m to 3.0 m by 0.5m increments. The study revealed that Small openings yield minor effects on the load capacity of shear walls, flexural stresses along the base level of shear walls, cracking pattern and maximum drifts. The larger the area of the opening is the extra is the stress flow disturbance within the shear wall. The study also conducted that when

openings are large enough, the load capacity is reduced because stiffness of shear wall with openings decreases.

Kankuntla et al. (2016) aimed to compare seismic performance of 15-Storey with openings in shear wall situated in earthquake zone V. Seismic coefficient method and Response spectrum method were used for seismic analysis. SAP software was used and the results were compared. Location of shear wall was determined by changing shape configuration and areas of openings in shear wall for all buildings models. The study concluded that, the presence of openings in shear wall decreases the strength and rigidity of the shear wall depending on the sizes and shapes of opening. The column moment and axial force is increased as sizes of opening increase because of reduction of stiffness of shear wall with openings. The opening effect decreases as length of shear wall in plan increases. Moreover, the responses of structure are not affected by shapes of opening but the width and height of openings have significant effect. The frames with shear wall is stricken by the size of openings than their positions inside the shear walls on the stiffness and response of structure with opening size ≤15% of solid shear wall area. However, it is extensively impacted by the opening positions in shear walls with opening area >15% of solid wall area.

Despite of the growing interest in modeling and analyzing behavior of shear walls, no researcher has yet seriously examined various parameters to have an optimum opening shape, orientation, aspect ratio, size, and position in RC wall, which could help designers in making openings either after construction or prior design. Consequently, by the use of ANSYS, the behavior of RC walls with openings can be explored. If the material properties have been implemented properly, ANSYS could simulate the elastic and plastic deformations that would take place in concrete till ultimately concrete crushing due to increasing the load.

Research Scope and Objective

The purpose of this study is to explore the behavior of shear walls with openings using finite element approach after being accurately verified experimentally and mathematically. The study includes a parametric study to gain an optimum opening shape, orientation, aspect ratio, size and position in R.C. wall with different thicknesses to increase capacity and dominance cracks. This paper is a part of a larger research study on the performance of opening configuration of shear wall openings and the use of fiber-reinforced polymers (FRPs) for strengthening those opening to enhance their behavior in opposing horizontal loads in high-rise buildings. The ongoing program is expected to significantly extend the findings of the previous studies and present a verified F.E. approach, which help for more research in this field. In addition, this paper conducts a new mathematical formula to predict the ultimate axial strength of the R.C. wall with circular opening.

Table 1. *Examined Parameters by F.E.M*

Serial No.	Shape	Vertical Dim.	Horizontal Dim.	Position	Wall Thickness (m)	Aspect Ratio	Opening size %
1	Square	0.4	0.4	Middle	0.06	1.00	6.58%
2	Square	0.4	0.4	Middle Right	0.06	1.00	6.58%
3	Square	0.4	0.4	Top Corner	0.06	1.00	6.58%
4	Square	0.4	0.4	Top Middle	0.06	1.00	6.58%
5	Square	0.4	0.4	Bottom Corner	0.06	1.00	6.58%
6	Square	0.4	0.4	Bottom Middle	0.06	1.00	6.58%
7	Square	0.6	0.6	Middle	0.06	1.00	14.81%
8	Square	0.6	0.6	Middle	0.09	1.00	14.81%
9	Square	0.6	0.6	Middle	0.12	1.00	14.81%
10	Square	0.6	0.6	Middle	0.15	1.00	14.81%
11	Square	0.6	0.6	Middle	0.18	1.00	14.81%
12	Square	0.6	0.6	Middle	0.21	1.00	14.81%
13	Square	0.6	0.6	Middle	0.24	1.00	14.81%
14	Square	0.6	0.6	Middle	0.27	1.00	14.81%
15	Square	0.8	0.8	Middle	0.06	1.00	26.34%
16	Square	1.0	1.0	Middle	0.06	1.00	41.15%
17	Square	1.2	1.2	Middle	0.06	1.00	59.26%
18	Rectangle	0.8	0.2	Middle	0.06	0.25	6.58%
19	Rectangle	0.2	0.8	Middle	0.06	4.00	6.58%
20	Rectangle	0.8	0.4	Middle	0.06	0.50	13.17%
21	Rectangle	0.4	0.8	Middle	0.06	2.00	13.17%
22	Rectangle	1	0.6	Middle	0.06	0.60	24.69%
23	Rectangle	0.6	1	Middle	0.06	1.67	24.69%
24	Rectangle	1	1.4	Middle	0.06	1.40	57.61%
25	Rectangle	0.4	1	Middle	0.06	2.50	16.46%
26	Rectangle	1	0.4	Middle	0.06	0.40	16.46%
27	Rectangle	0.8	0.6	Middle	0.06	0.75	19.75%
28	Rectangle	0.8	0.6	Middle	0.09	0.75	19.75%
29	Rectangle	0.8	0.6	Middle	0.12	0.75	19.75%
30	Rectangle	0.8	0.6	Middle	0.15	0.75	19.75%
31	Rectangle	0.8	0.6	Middle	0.18	0.75	19.75%
32	Rectangle	0.8	0.6	Middle	0.21	0.75	19.75%
33	Rectangle	0.8	0.6	Middle	0.24	0.75	19.75%
34	Rectangle	0.8	0.6	Middle	0.27	0.75	19.75%
35	Rectangle	0.6	0.8	Middle	0.06	1.33	19.75%
36	Rectangle	0.4	1.2	Middle	0.06	3.00	19.75%
37	Rectangle	0.5	0.8	Middle	0.06	1.60	16.46%
38	Rectangle	0.3	1.2	Middle	0.06	4.00	14.81%
39	Rectangle	0.5	1	Middle	0.06	2.00	20.58%
40	Rectangle	0.7	0.8	Middle	0.06	1.14	23.05%
41	Rectangle	0.5	1.2	Middle	0.06	2.40	24.69%
42	Rectangle	0.5	0.6	Middle	0.06	1.20	12.35%
43	Rectangle	0.3	0.6	Middle	0.06	2.00	7.41%
44	Rectangle	0.3	1.4	Middle	0.06	4.67	17.28%
45	Rectangle	0.3	1.4	Middle	0.06	4.67	17.28%
46	Rectangle	0.3	0.8	Middle	0.06	2.67	9.88%
47	Rectangle	0.4	0.6	Middle	0.06	1.50	9.88%
48	Rectangle	0.2	1.2	Middle	0.06	6.00	9.88%
49	Rectangle	0.3	1	Middle	0.06	3.33	12.35%

50	Rectangle	0.2	1.4	Middle	0.06	7.00	11.52%
51	Rectangle	0.7	0.4	Middle	0.06	0.57	11.52%
52	Rectangle	0.5	0.4	Middle	0.06	0.80	8.23%
53	Rectangle	0.6	0.4	Middle	0.06	0.67	9.88%
54	Rectangle	1.2	0.2	Middle	0.06	0.17	9.88%
55	Rectangle	0.2	0.4	Middle	0.06	2.00	3.29%
56	Rectangle	0.6	1.2	Middle	0.06	2.00	29.63%
57	Circular	Diameter	0.8	Middle	0.06	-	20.67%
58	Circular	Diameter	0.6	Middle	0.06	-	11.63%
59	Circular	Diameter	0.7	Middle	0.06	-	15.83%
60	Circular	Diameter	0.5	Middle	0.06	-	8.08%
61	Circular	Diameter	0.9	Middle	0.06	-	26.17%
62	Circular	Diameter	0.45	Middle	0.06	-	6.54%

Methodology

The research plan includes three phases, the first phase; includes verification of the experimental results conducted by other researchers using an ANSYS model and ensure the correlation between both F.E. and experimental results for load capacity, failure mode and lateral displacement. The research depends on two different experimental programs using three different F.E models to be more confident with the model results.

The second phase; After the model has been verified with the experimental outputs, a parametric study has been conducted by changing opening shape, opening location, size of opening, aspect ratio of opening, rectangular opening orientation and changing R.C. wall thickness. Table 1 shows the details of the examined parameters and its variation. So that a number of 62 different F.E. model have been conducted on ANSYS for such study.

The third phase includes verification between the F.E approach and other mathematical design models. Then, a statistical analysis is performed on 38 F.E. specimens to validate the accuracy of the current mathematical design models. Based on the results of this statistical analysis, an overview is provided on the performance of current design models and to identify research gaps. The results will be used to conduct a new mathematical formula to get the ultimate axial load of R.C wall with circular opening.

Finite Element Analysis of Shear Wall with Openings

ANSYS finite element software is used to model two experimental programs of reinforced concrete shear loaded in the model up to failure, which have a symmetric opening (Popescu et al. 2016) and (Mohammed et al. 2010). Nonlinear response of RC wall is developed by cracking, plastic deformations in compression, crushing of the concrete and plastic deformations of the reinforcement.

Experimental Data Used for Model Verification
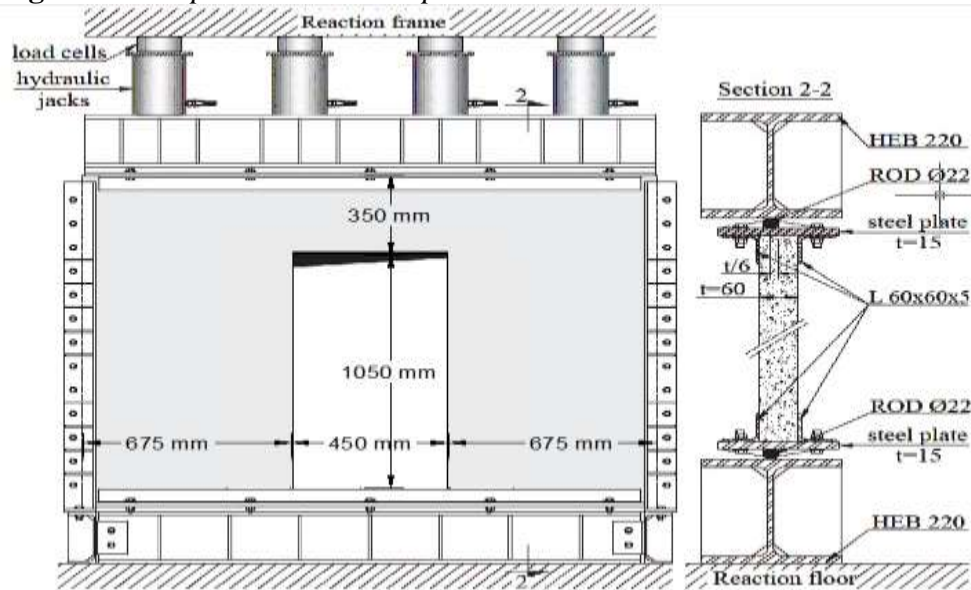
<u>First Model Verification</u>

Two shear wall specimens named I-L and I-S designed to represent typical wall panels in residential buildings (1800mm long, 1350mm tall and 60mm thick), modeled for testing to failure, they have symmetric openings (900mm x 1050mm) & (450mm x 1050mm) as shown in Figures 1 and 2. The specimens are designed to be load-bearing concrete walls that are loaded by vertical loads with no transverse loads between supports or lateral in-plane forces. Welded wire fabric reinforcement was used to reinforce the walls, comprising of deformed 5 mm diameter bars with 100 mm spacing in both orthogonal directions and centrally positioned in a single layer. The concrete utilized to cast the specimens was a self-consolidating blend that could be poured without vibrating it. The average cubic compressive strength of the concrete was 62.8 MPa. Steel mean yield strength (fy) was 632MPa.

Four hydraulic jacks, each with a most extreme limit of 1400kN, were connected together to apply a uniformly distributed load, with controlled total force, along the wall length. An eccentricity of one sixth of the wall thickness was applied in the loading. A steel rod was welded to both of loading beam in order to apply eccentric distributed loading, designed to fit into a guide system connected to the upper edge and lower edge of the specimen as illustrated in Figure 1 and 2 (Popescu et al. 2016).

**Figure 1.** *I-L Specimen Test Setup*
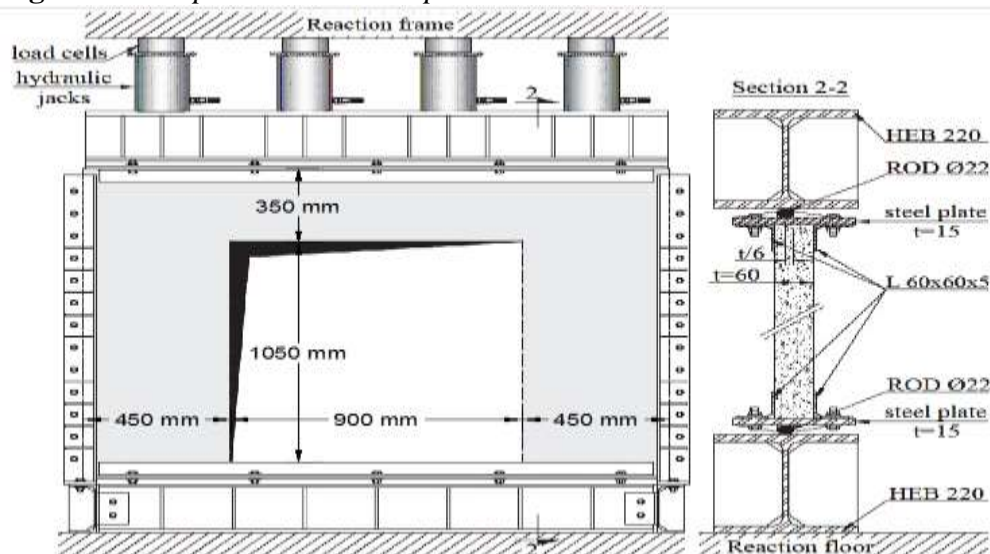
Figure 2. *I-S Specimen Test Setup*

Second Model Verification

A shear wall specimen named WO2 designed to represent typical wall (400mm long, 800mm tall and 50mm thick), modeled for testing to failure, it has a symmetric opening (135mm x 240mm) as shown in Figure 3. The specimen was cast with constant thickness. The specimen is designed to be a load-bearing concrete wall that is loaded by vertical loads with no transverse loads between supports or lateral in-plane forces. Welded wire fabric reinforcement was used to reinforce the walls, consisting of deformed 5 mm diameter bars and centrally positioned in a single layer. The concrete used to cast the specimens was a self-consolidating blend that could be poured without vibrating it. The average cubic compressive strength of the concrete was 22.11 MPa. Steel mean yield strength (f_y) was 478MPa.

A hydraulic jack with a most extreme limit of 300kN, applies a uniformly distributed load, with controlled total force, along the wall length. An eccentricity of one sixth of the wall thickness was applied in the loading. A steel rod was welded to both of loading beam in order to apply eccentric distributed loading, designed to fit into a guide system connected to the upper edge and lower edge of the specimen as illustrated in Figure 3 (Mohammed et al. 2010).

Figure 3. *Test Setup of WO2 Specimen* (Mohammed et al. 2010)
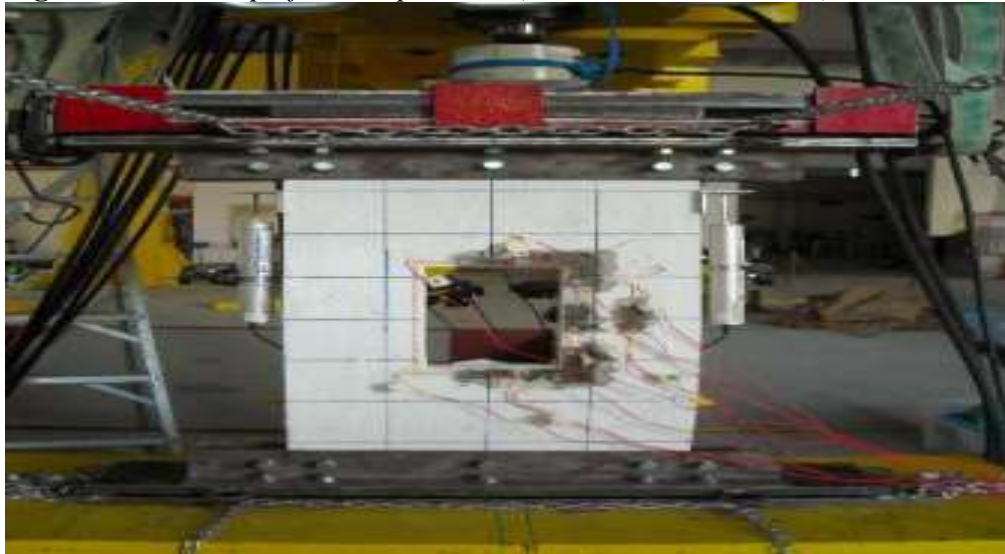
Material Model

Modeling of Concrete

The nonlinear response of reinforced concrete is modeled by solid65 element. The concrete material is modeled by this element, which primarily based on a constitutive model for the triaxial behavior of concrete after Williams and Warnke (1975). This element is isoperimetric element which is characterized by eight nodes, each having three translation degrees of freedom in the nodal x,y and z-directions. The geometry, node positions and the coordinate system for the element is appeared in Figure 4. It is able to simulate plastic and elastic deformation, crushing in compression and cracking in tension in three perpendicular directions at each integration point as the load is increased (Morsy et al. 2015).

Figure 4. *Solid 65 Element*
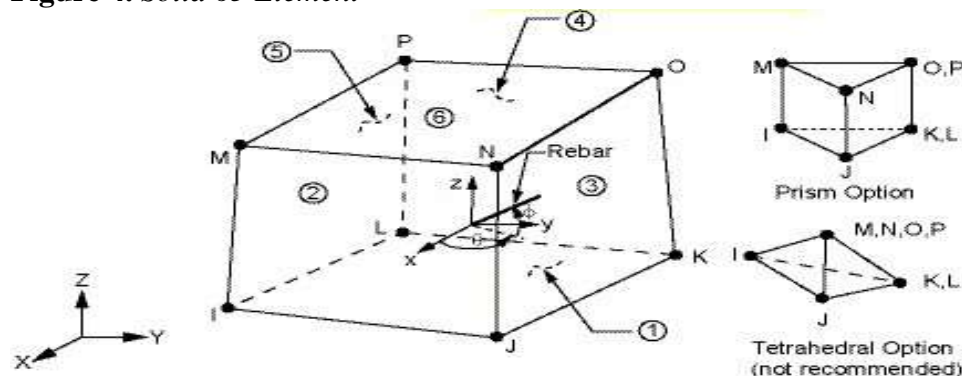
Changing the element stiffness matrices conducts an adjustment in the material properties, which helps in the cracking modeling. In Solid 65,

crushing is known as the complete deterioration of the structural integrity of the material (material spalling). If the material fails at an integration point in uniaxial, biaxial or triaxial compression, the material is assumed to be crushed at that point. The von Mises failure criterion is used to model the multi-linear isotropic concrete along with Willam and Warnke model to define the failure of concrete.

The multi-linear isotropic stress-strain curve for the concrete is computed by the use of the following equations (Chinese Standard, 2002)[3] & Rusch model (Rusch and Hilsdorf 1963) in order to obtain the compressive uniaxial stress-strain relationship for the concrete model.

When fcu > 50 MPa

$$\sigma_c = f_c \left[1 - \left(1 - \frac{\varepsilon_c}{\varepsilon_0} \right)^n \right] \quad \varepsilon_c \leqslant \varepsilon_0$$
$$\sigma_c = f_c \quad \varepsilon_0 < \varepsilon_c \leqslant \varepsilon_{cu}$$

$$n = 2 - \frac{1}{60}(f_{cu} - 50)$$

$$\varepsilon_0 = 0.002 + 0.5(f_{cu} - 50) \times 10^{-5}$$

$$\varepsilon_{cu} = 0.0033 - (f_{cu} - 50) \times 10^{-5}$$

When fcu < 50 MPa

$$\sigma_c = f_c \left[2\frac{\varepsilon_c}{\varepsilon_0} - \left(\frac{\varepsilon_c}{\varepsilon_0} \right)^2 \right] \quad (\varepsilon_c \leqslant \varepsilon_0)$$

$$\sigma_c = f_c \quad (\varepsilon_0 < \varepsilon_c \leqslant \varepsilon_{cu})$$

Where:
σ_c: the stress in concrete corresponding to the compressive strain ε_c
f_c: the axial compressive strength of concrete
ε_o: the compressive strain corresponding to f_c
ε_{cu}: the ultimate compressive strain
f_{cu}: the cube strength of concrete
n: a parameter

Table 2. *Concrete Properties prior to Initial Yield Surface*

	1st experimental program	2nd experimental program
Modulus of elasticity "MPa"	41236.18	16761.59
Poisson's ratio	0.2	0.2
Shear transfer coefficients for an open crack (βt)	0.5	0.5
Shear transfer coefficients for a closed crack (βc)	1	1
Uniaxial tensile cracking stress (fr) "MPa"	6.28	2.21
Uniaxial crushing stress (fc) "MPa"	62.8	22.11

States of the crack face is represented by the shear transfer coefficient β. β starts from 0 to 1, with 0 indicating a smooth crack (complete loss of shear transfer) and 1 indicating a rough crack (no loss of shear transfer) (Kwan et al.

---

[3] Chinese Standard 'GB 50010-2002' (2002) *Code for Design of Concrete Structures.*

1999, Terec et al. 2010). Table 2 lists concrete properties within Solid65 element.

Modeling of Steel Reinforcement

The link8 element models the nonlinear response of reinforcement bars which may be included in the finite element model as a discrete model (individual bars). As shown in Figure 5, prior to initial yield surface steel material model is linear elastic, after the initial yield surface it is completely plastic, in compression and tension loading. Figure 6 shows the geometry, node positions and the coordinate system for the element. The parameters selected to define the material properties of steel are given in Table 3.

Table 3. *Material Properties for Steel*

Linear Isotropic		
Es "MPa"	200000	
Poisson's ratio	0.3	
Bilinear Isotropic		
	1st experimental program	2nd experimental program
Yield Stress "MPa"	632	478
Tang Modulus "MPa"	632	478

Figure 5. *Stress-Strain Curve for Steel Reinforcement*
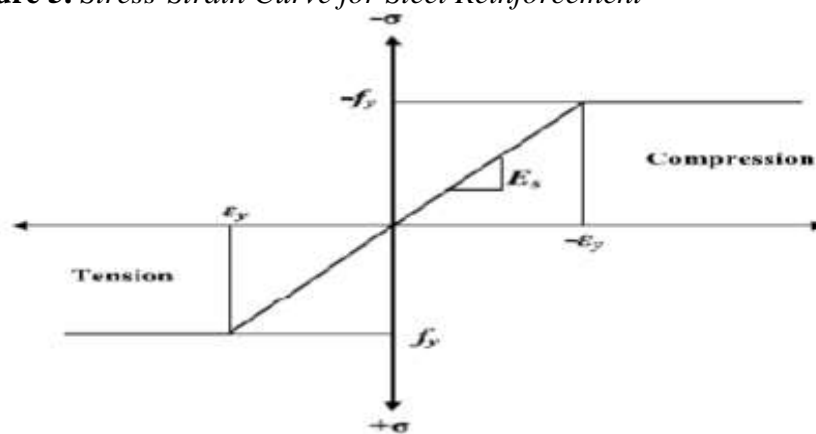

Figure 6. *Link8 Element*

Meshing & Load Steps

The mesh generation directly affects the accuracy of F.E. analysis results. The mesh generation method is mainly determined by the element type and shape. Perfect simulation needs highly refined meshes.

The panels are meshed with specific material characteristics by using 8-node elements called Solid 65 for concrete, link 8 for reinforcement steel and solid 185 for loading plates. A dense mesh of this element type may be required in order to obtain accurate results during the analysis. ANSYS parametric design language (APDL) generates the mesh. In this method of mesh generation, the nodes are assigned to specific coordinates with ordered numbering. Then, meshed elements are formed after the nodes are joined together. The accuracy of the model, including objectivity issues related to mesh geometry and size, is demonstrated through several mesh sensitive studies, which were performed to select the optimum mesh sizes. In the models of first experimental program, the elements have a length of 50 mm. Elements have a length of 25 mm in the second experimental program. In the specimen named I-L in the first experimental program, there are 4620 nodes in the model, which are connected together to form 4068 elements as shown in Figure 7. Specimen named I-S in the first experimental program, there are 5000 nodes in the model, which are connected together to form 4464 elements. Concerning the second experimental program, there are 2750 nodes in the model, which are connected together to form 2170 elements.

**Figure 7.** *Meshed Elements*
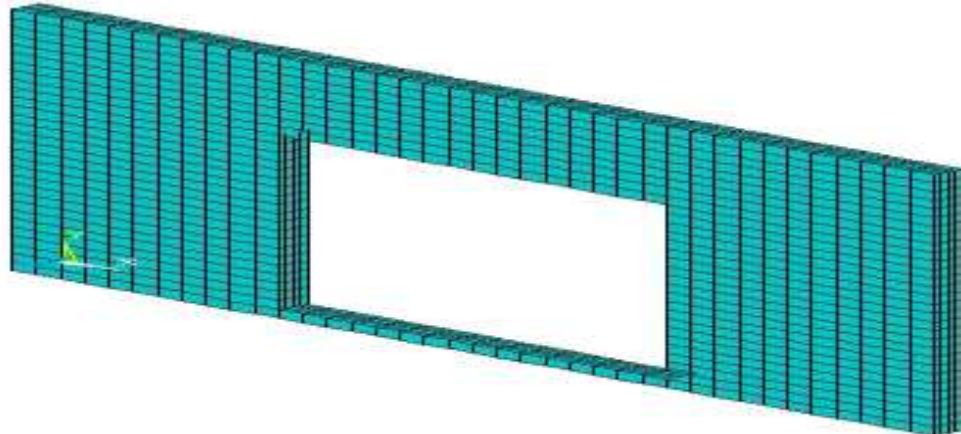
Automatic time stepping was used to solve the FE model with a specific number of substeps (1000) depending on the material properties, the value of loads and element density. In order to carry out a load-displacement curve based on non-linear analysis in ANSYS, the load should be broken into a series of load increments by defining number of load steps (185) in the first experimental program and (60) in the second experimental program, increment in load to be applied in each step and maximum load to be applied. The model

must be always checked back to determine the exact load step at which the wall failed.

Loading and Boundary Condition

Hinged connections at the top and bottom boundaries of the specimen and clamped side edges, which had to be sufficiently rigid to stop immoderate out-of-plane deformations. Top edge is restrained in x and z directions along the wall length and released in y direction which is the loading direction. Bottom edge is restrained in x, y and z directions along the wall length. Side edges are restrained in x and z directions along the wall height in the first experimental program but released in all directions in the second experimental program. In order to simulate what happens in the laboratory properly, an axially uniformly distributed load is applied in the F.E.M. along the wall length with a small eccentricity at both of upper and lower end (one sixth of the wall thickness) to emulate influences of defects that happen in ordinary construction practices as presented in Figure 8. In the first experimental program, the model is axially loaded by distributed load of 5000kN by applying pressure 185Mpa along the wall length and 15 mm width. That load almost simulates the actual loading process developed in the laboratory as the wall loaded by four hydraulic jacks, each with a most extreme limit of 1400kN. These jacks were connected together to apply a uniformly distributed load, with controlled total force along the wall length. In the second experimental program, the model is axially loaded by distributed load of 300kN by applying pressure 60Mpa along the wall length and 12.5mm width. That load almost simulates the actual loading process developed in the laboratory as the wall loaded by one hydraulic jack with a maximum capacity of 300kN. When the model also has been loaded with different loads more than the expected failure load, it is found that the model failed at the same failure load, which ensures the F.E. model accuracy.

Figure 8. *Applied Load*
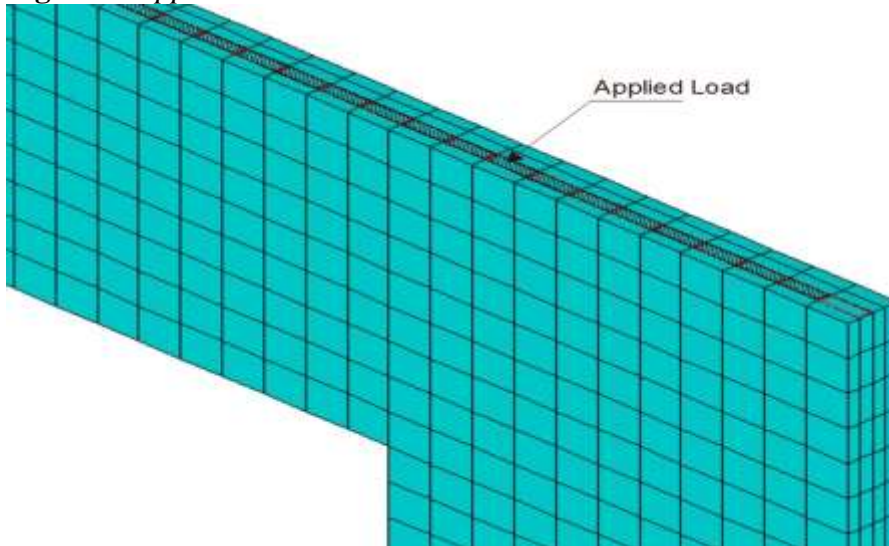
Failure Criteria

In this research, failure is considered when steel reinforcement yields followed by severe cracking of concrete. This initiates a large disturbance to the FE simulation and a major difficulty to the solution algorithm. This in turn leads to termination in the FE simulation due to a divergence. Divergence in the FE solution corresponds with an extremely large deflection, surpassing the displacement limitation of the ANSYS software.

Model Verification

F.E. modeling approach has been conducted and verified with two experimental programs of three different specimens conducted by Cosmin Popescu et al. (2016) and Mohammed et al. (2010). After verification, a parametric study is applied to investigate the effect of opening size, shape, orientation, aspect ratio, position with different R.C. wall thicknesses.

Verification of First Experimental Program

Verification for Load versus Deformation Curve

The validity of the proposed material constitutive models for steel and concrete were verified by comparing their predictions with experimental data conducted from testing reinforced concrete shear wall (1800mm long, 1350mm tall and 60mm thick and has a symmetric opening (900mm x 1050mm) which named I-L. The results of the verification study, Figure 9, demonstrated that the F.E. model fitted with the experimental results of the reference wall. The measured maximum capacity and corresponding out of plane displacement in the reference wall were 1180kN and 12mm, respectively. On the other hand, the F.E. predictions obtained for maximum capacity and corresponding out of plane displacement were 1240kN and 12.9mm, respectively.

Another specimen has been conducted for verification, which has a symmetric opening (450mm x 1050mm) and named I-S. The results shown in Figure 9 demonstrated that the F.E. model fitted with acceptable accuracy the experimental results of the reference wall. The measured maximum capacity and corresponding out of plane displacement in the reference wall were 1500kN and 15.5mm, respectively. On the other hand, the F.E. predictions obtained for maximum capacity and corresponding out of plane displacement were 1780kN and 13mm, respectively. The experimental and F.E. failure loads and out of plane displacement capacities are presented in Table 4.
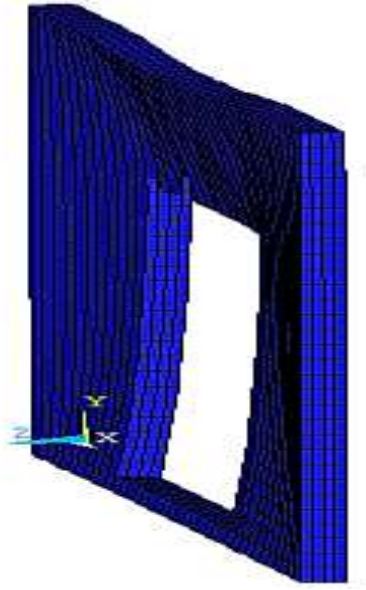
Table 4. *F.E. and Experimental Results*

Serial	Ultimate load, Pu (kN)			Out of plane displacement (mm)		
	Anal.	Exp.	Accuracy %	Anal.	Exp.	Accuracy %
I-L	1240	1180	5.1	12.9	12	7.5
I-S	1605	1500	7.0	15.6	15.5	0.64

Figure 9. *Exp. and F.E. Results for I-L & I-S Specimens*
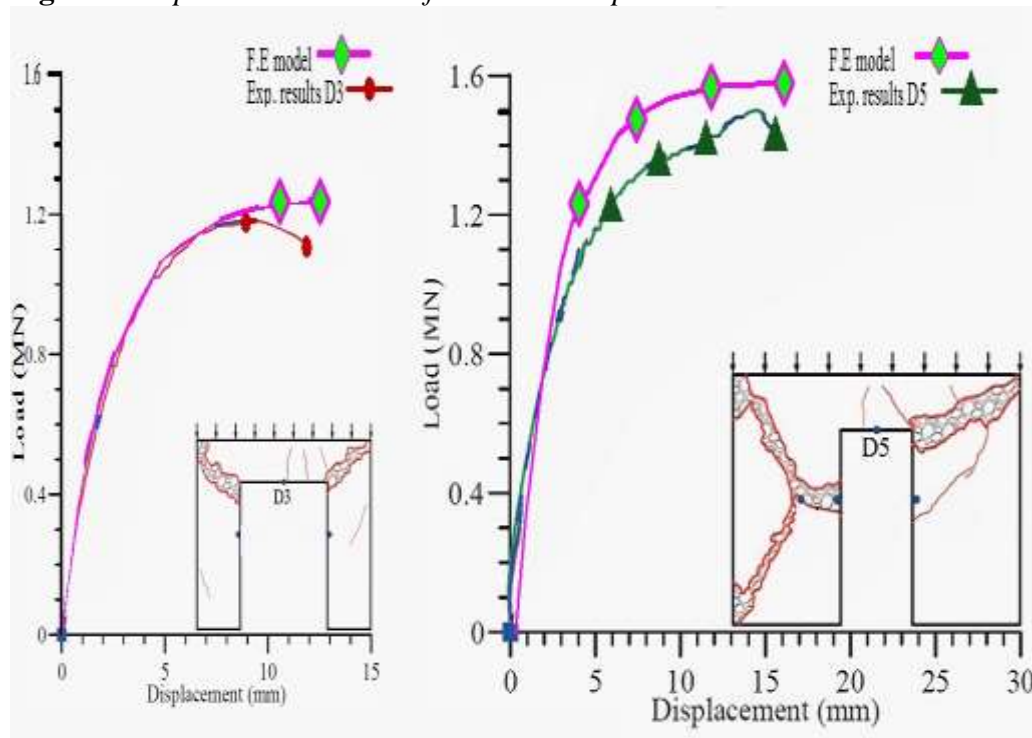
Crack Pattern and Failure Mode

The specimen I-L failed in a mode of deflection in a single curvature with a maximum deflection occurring near the middle of the wall panel as shown in Figure 10. Crack Propagation is shown in Figure 11. The brittle failure in the wall caused by crushing of concrete with spalling and reinforcement buckling along the line between the opening corner and wall corner of one pier which leads to the failure of the wall panel as illustrated in Figure 12. Comparing the crack pattern of sample specimen at failure predicted numerically to that obtained from the experiment in Figure 12, there is a good correlation between the experimental and F.E. crack patterns.

Figure 10. *Deformed Shape for I-L*   **Figure 11.** *Crack Propagation for I-L*
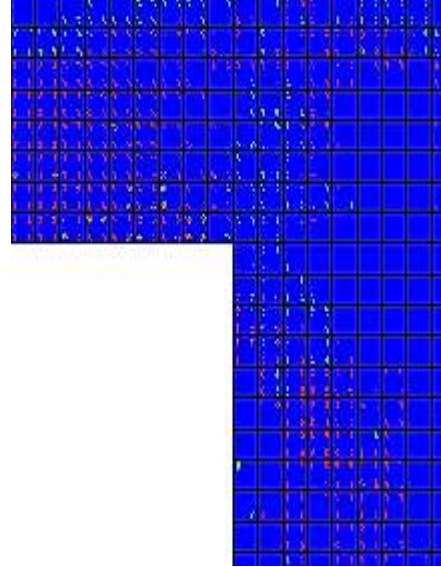
Figure 12. *Cracks in Experimental Specimen for I-L*

The specimen I-S failed in a mode of deflection in a single curvature with a maximum deflection occurring near the middle of the wall panel as shown in Figure 13. Cracks opened along the line between the corner of the wall and opening corner and these cracks continued to widen when several other cracks around the same location began to grow. The brittle failure in the wall caused by crushing of concrete with spalling and reinforcement buckling along the line between the opening corner and wall corner of one pier (Figure 14). Comparing the crack pattern of sample specimen at failure predicted numerically to that obtained from the experiment in Figure 15, there is a good correlation between the experimental and F.E. crack patterns.

Figure 13. *Deformed Shape for I-S*   **Figure 14.** *Crack Propagation for I-S*
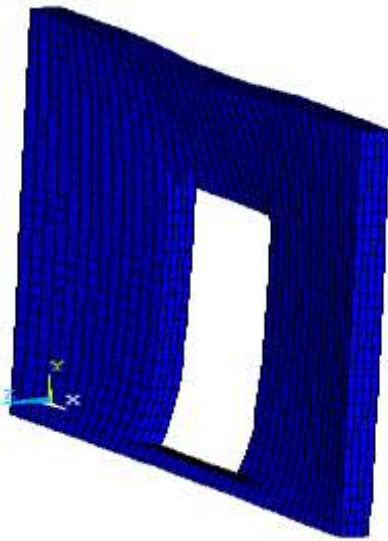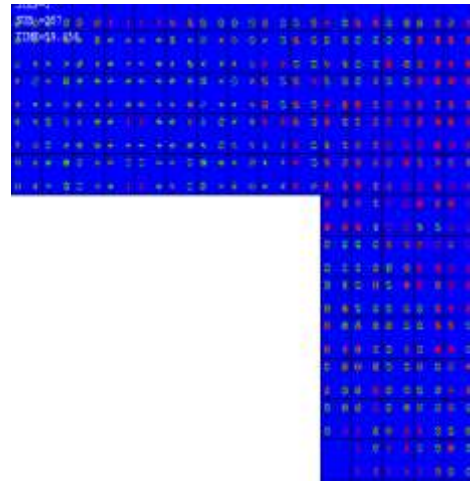
Figure 15. *Cracks in Experimental Specimen for I- S*
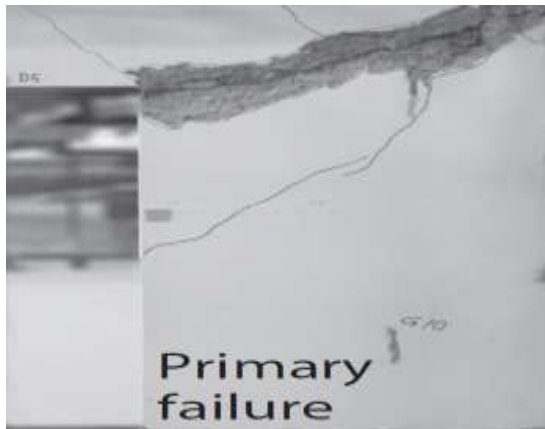
Verification for Second Experimental Program

<u>Verification for Load Capacity</u>

Proposed material constitutive models for steel and concrete were verified by comparing their predictions with another experimental data conducted from testing reinforced concrete shear wall (Mohammed et al. 2010). The reference wall dimensions were (400mm long, 800mm tall and 50mm thick and has a symmetric opening (240mm x 135mm) which named WO2 as illustrated in Figure 3. The results of the verification study demonstrated that the F.E. model fitted with the experimental results of the reference wall. The measured maximum capacity in the reference wall was 203.8kN. On the other hand, the F.E. predictions obtained for maximum capacity was 175.12kN with 16.4% variation.

Crack Pattern and Failure Mode

The specimen WO2 fails in a mode of deflection in a single curvature with a maximum deflection happening close to the middle of the wall panel as illustrated in Figure 16. The cracks begin from the center of the opening, parallel with the loading direction towards the applied loads. Followed by that is a crack from the center of the opening, parallel with the loading direction towards the bottom of the wall panel. Other than that, the cracks also happened near the middle of the wall panel, orthogonal to the loading direction, which causes the failure of the wall panel as appeared in Figure 17. Comparing the crack pattern of sample specimen at failure predicted numerically to that obtained from the experiment in Figure 18, there is a good correlation between the experimental and F.E. crack patterns.

Figure 16. *Deformed Shape*   **Figure 17.** *Crack Propagation*

At Load 70kN   At Load 154kN
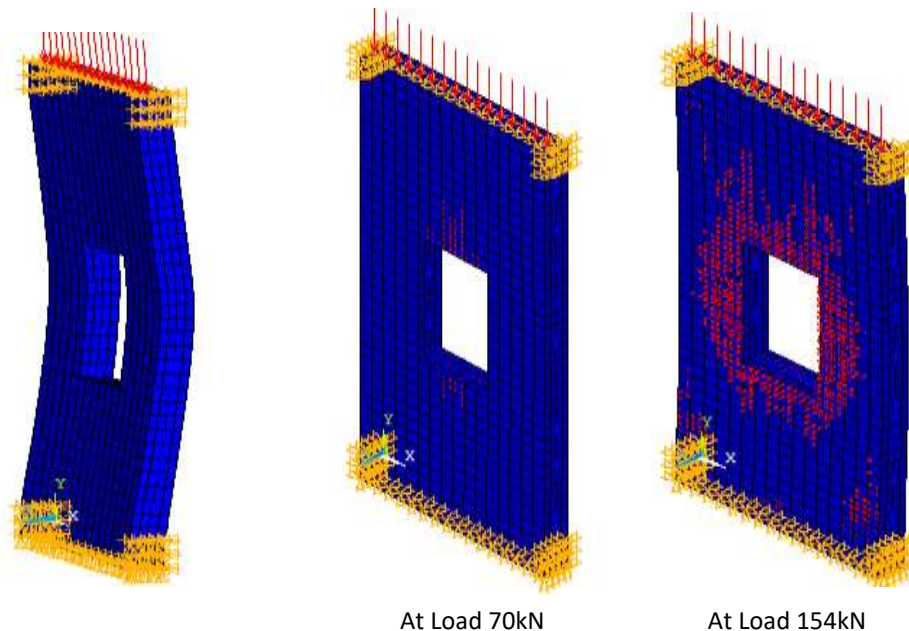
Figure 18. *Cracks in Experimental Specimen*

Failure mode in the F.E. models fitted with the experimental results of the reference walls, which confirms the capability of the F.E. models to accurately predict the load capacity of other models of shear walls and simulate the nonlinear structural behavior of opened shear walls to examine a larger domain of parameters instead of laboratory testing, which is expensive, time-consuming and labor-dense. After verification of the finite element method with the proposed reference models, several arrangements of openings with a variety of dimensions were created in different shapes in the reference wall model to examine the impacts of openings.

Parametric Study

Effect of Opening Shape

Based on the F.E. study carried out on four shapes with the same average opening size and position, it is clearly seen that the opening shape has significant impact on the axial capacity values at failure stage. The square shape has the lowest carrying capacity then the circular shape is much higher and the maximum axial load capacity is related to R.C wall with vertical rectangle direction opening. As shown in Table 5, it can be noticed that for a constant average value of opening size 15.9% of the total wall area, which located in the middle, the lowest ultimate load is recorded at square shape, which is 1630.8kN, then the circular shape with 1695.6kN. Meanwhile, the ultimate load of wall with vertical rectangle direction opening reaches 2155.68kN which is slightly lower than the solid wall capacity by 8.8%. Therefore, the highest load capacity is related to vertical rectangle direction and these findings indicate that the effect of changing the opening shape should not be ignored. The main reason is that the loaded cross section area at opening section in the R.C wall with vertical rectangle opening is larger than those in the other shapes at the same opening section. This large area can resist higher axial load values.

Regarding the stress concentration, the presence of the openings in the panels determines the load paths and creates high stress concentrations around the opening, which encourages cracks to occur first at the corners of the opening. Therefore, the circular openings are preferred as there are no corners & concentrations, which cause lower stress values around the opening than other shapes as shown in (Figure 19).

Table 5. *Changing Opening Shape Results*

Shape Sr.	Opening Shape	Vertical dim. (m)	Horizontal dim. (m)	Average Opening Area %	Load (kN)	Shape	Capacity reduction than solid wall %
Solid wall	No opening	———	———	———	2363	——	———
1	Rectangle	1	0.4	15.9%	2155.7		8.8%
2	Circular	Dia. =	0.7	15.9%	1695.6		28.2 %
3	Square	0.6	0.6	15.9%	1630.8		31 %

Figure 19. *Stress Concentration in Different Shapes*
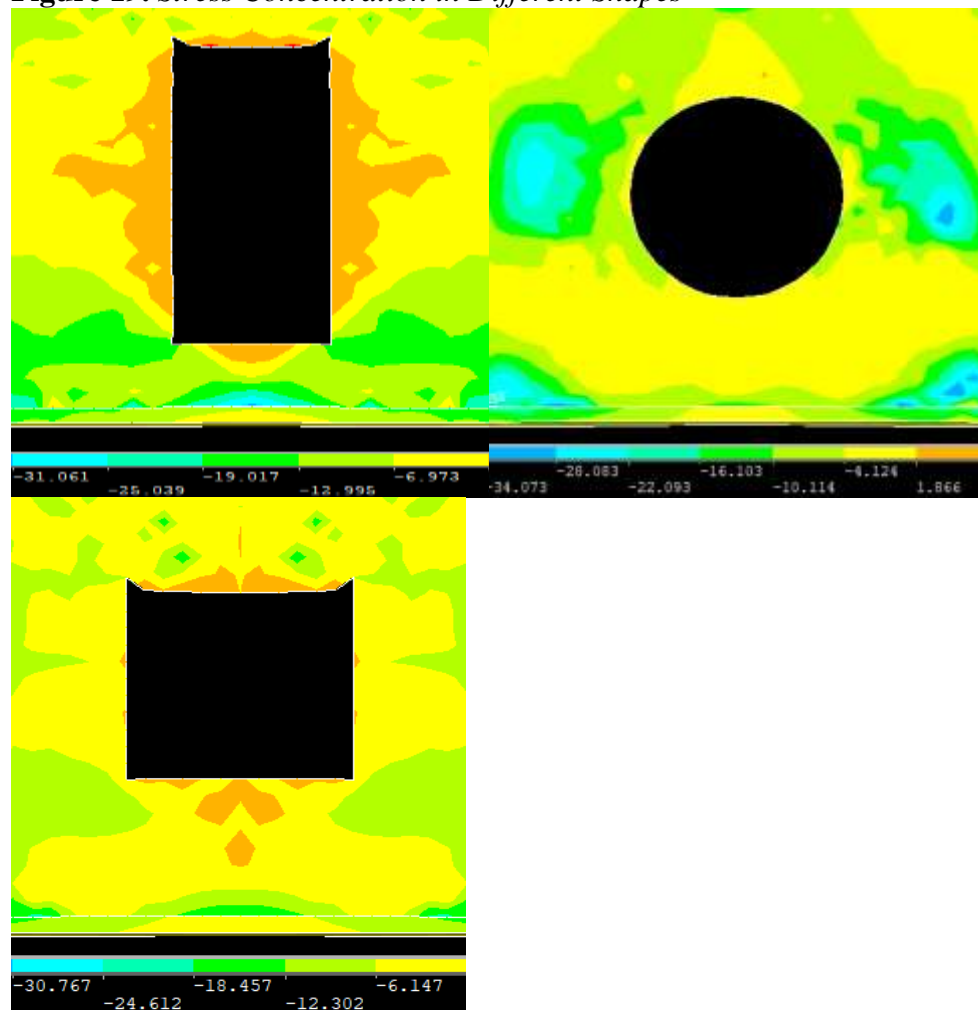
Effect of Opening Orientation

F.E. study's findings conducted that changing rectangle orientation has considerable effects on the axial capacity. The F.E. study is carried out on two different groups in terms of aspect ratio. Both of the groups have the same size and locate in the middle of the wall. The opening orientation is varying in the same group from horizontal direction to vertical direction and opening area is constant for both of groups (10% of the total wall area). Results of Groups G1 (aspect ratio = 1.5) and G2 (aspect ratio = 6) were analyzed to demonstrate the effect of opening orientation on RC walls behavior. The enhancement in axial capacity increases when the rectangular opening is in vertical direction because the loaded cross section area at the opening section in the R.C wall with vertical rectangle opening is larger than the loaded cross section area in the R.C wall with horizontal rectangle opening at the same opening section as shown in Table 6. When the solid wall axial capacity compared with G1 rectangular opening in vertical direction, it can be noticed that the ultimate axial load value decreases by 1% unlike the horizontal rectangle direction that records 1719.9kN with 27.2% reduction. G2 follows the same manner of G1 as vertical rectangular direction opening ultimate axial load decreases by 7.3% counter to the horizontal rectangle direction, which records 772.2kN with 67.3% reduction. It can be also noticed that when the aspect ratio decreases, the difference in ultimate load value between the two shapes decreases. According to the table, in G1, the difference in ultimate load value was about 621kN. On the other hand, the aspect ratio was 6 in G2 and that significant change reflected in difference in ultimate load value which was 1418.6kN. In addition, it can be seen that when rectangular opening is in vertical direction, the out of plane displacement values increase. The out of plane displacement here defines and indicates the ductility. When the out of plane displacement value increases, the ductility of the R.C. wall increases. As shown in Table 6, it can be noticed that for G1 and G2, the out of plane displacement for vertical rectangle direction are 20.01 & 15.72mm, which are more than horizontal rectangle direction values 16.23 and 4.8mm respectively. These displacement values indicate that rotation from horizontal rectangle direction to vertical rectangle direction increases the wall ductility. It is obviously concluded that the changing the opening orientation has considerable impact on the wall ductility and the axial capacity values.

Table 6. *Changing Opening Orientation Results*

Group	Ver. Dim. (m)	Hor. Dim. (m)	Aspect ratio	Orientation	Load kN	Capacity reduction than solid wall %	Out of plane Dis. (mm)
Solid	——	——	——	——	2363	——	22.5
G1	0.6	0.4	1.50		2340.9	1%	20.01
	0.4	0.6			1719.9	27.2%	16.23
G2	1.2	0.2	6.00		2350.4	0.5%	15.72
	0.2	1.2			772.2	67.3%	4.80

Effect of Opening Aspect Ratio

FE models illustrated that opening aspect ratio has significant impact on the axial load capacity of R.C walls. From Figure 20, it can be seen that when aspect ratio of middle horizontal rectangle direction opening is increased, the axial load capacity of the shear wall decreases because of the reduction in the resisting cross section area in the R.C. wall. While studying opening sizes 10.97%, 15.14% and 19.34% of the total wall area, it can be noticed that the reduction percentage in the solid wall ultimate load of aspect ratio 1 is (29%) which shows better results when compared to aspect ratio 2 (43.2%). The reduction percentage at aspect ratio 3 (58.4%) is lower than aspect ratio 4 which recorded the highest reduction percentage in the solid wall ultimate load (65%).

Figure 20. *Aspect Ratio versus Capacity Diagrams*
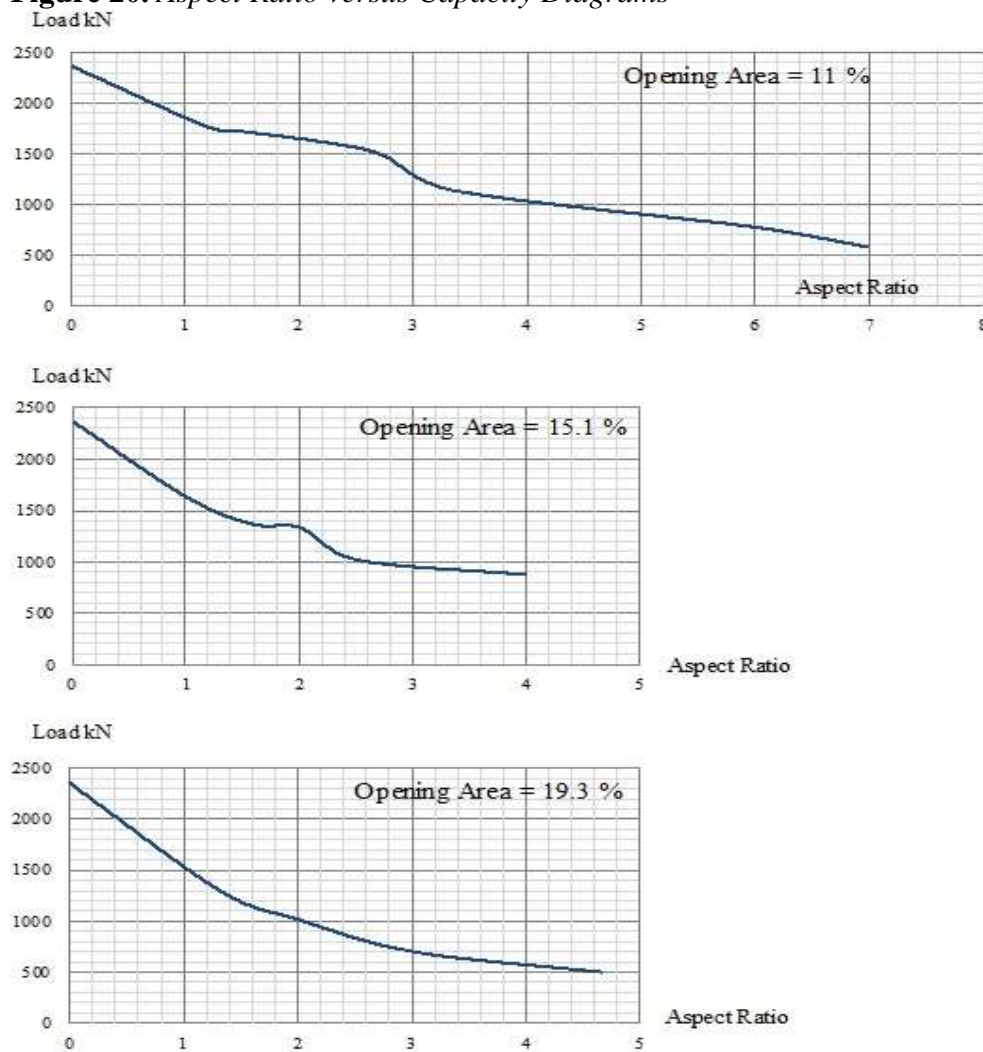
Effect of Opening Position

Figure 21 shows the positions of openings in the R.C. wall. The FE models in Table 7 conducted that the highest axial load capacity values at openings located at bottom of the shear wall because this position is away from the loaded edge and the axial load path. Then followed by lower load capacity values are recorded for the models with openings in the middle of the shear walls. In contrast, while the openings located at the top of the shear wall, the ultimate axial load value decreased sharply to be the lowest.

In addition, it can be noticed that when opening is shifted from the middle to edges and corners, the ultimate axial load values become lower than those in the middle. For example, in Table 7, it can be seen that for a constant value of opening size (6.58% of the total wall area) and constant shape (square), the ultimate load of position 2 is 2281.5kN which shows better results when compared to position 3 and slightly lower than position 1 which recorded the

highest axial capacity (2334.15) and the lowest reduction percentage from the solid wall capacity (1.22%).

Figure 21. *Positions of Opening in R.C Wall*
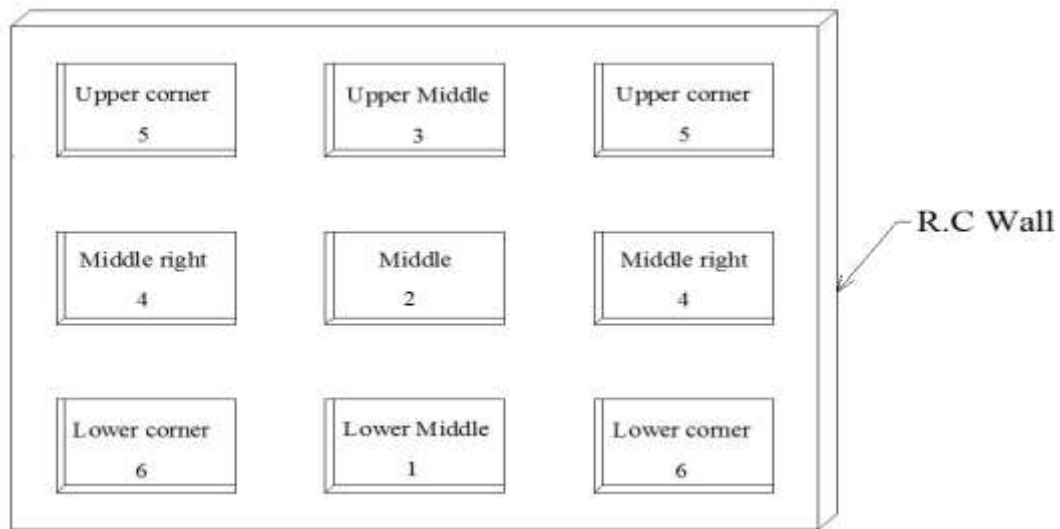
Shifting the opening position from position 1 to position 4 has displayed decreasing in the ultimate axial load value by 9%. The reduction in capacity from solid wall rose up from 1.22% to 12.13%. Another noticeable feature is that the highest out of plane displacement is corresponded to position 2, which is 20.05mm.

This leads us to believe that the best opening position in the shear wall in terms of axial load capacity is at the lower side in the middle (position 1) and in terms of ductility is at exact middle of the shear wall (position 2).

Table 7. *Changing Opening Position Results*

Position Sr.	Position	Ver. Dim. (m)	Hor. Dim. (m)	Load kN	Capacity reduction than solid wall %	Out of plane Dis. (mm)
Solid	———	——	——	2363	———	22
1	Lower Middle	0.4	0.4	2334.2	1.22%	10.73
2	Middle	0.4	0.4	2281.5	3.45%	20.05
3	Upper Middle	0.4	0.4	1657.8	29.8%	5.9
4	Middle Right	0.4	0.4	2076.3	12.13%	9.33
5	Upper Corner	0.4	0.4	1117.8	52.7%	9.3
6	Lower Corner	0.4	0.4	2206.2	6.6%	9.35

Effect of Opening Size

Opening size is highly affecting the axial capacity of R.C wall. Figure 22 briefly summarizes results for various models, which have the four shapes (vertical rectangle direction, circular, square and horizontal rectangle direction) and the same position (middle) & aspect ratio but have different sizes. The ultimate axial loads are presented in Figure 23 in the vertical axe and opening sizes are presented in the horizontal axe. The load-size curve indicates that minor effects on ultimate axial load are yielded for the shear wall with opening area less than 7% of the whole wall area. That almost accomplishes with guidelines provided in AS3600 (2009) and EN 1992-1-1 (2004) which state that if the walls are restrained on all sides and enclose an opening with an area less than 1/10 of the total, the effects of this opening on the axial strength can be neglected. Another noticeable feature is that when openings are large enough and exceed 7% of the whole wall area, the axial load capacity of the shear wall becomes less. According to the graph, the load capacity of circular shape went down to about 84.4% from 2352kN to 1275.48kN as we move from opening size 7% to 26.2%. Additionally, the opening area has extensive impact on out of plane displacement values of the shear wall as presented in table 8 for circular shape as an example. However, the out of plane displacement is reduced considerably as the opening size increases. The major conclusion that has been drawn is that small openings (size < 7%) have negligible effect on shear wall capacity. In contrast, the larger the size of the opening, the lower is the amount of shear wall capacity and ductility.

Figure 22. *Load-size Relationship Curve*
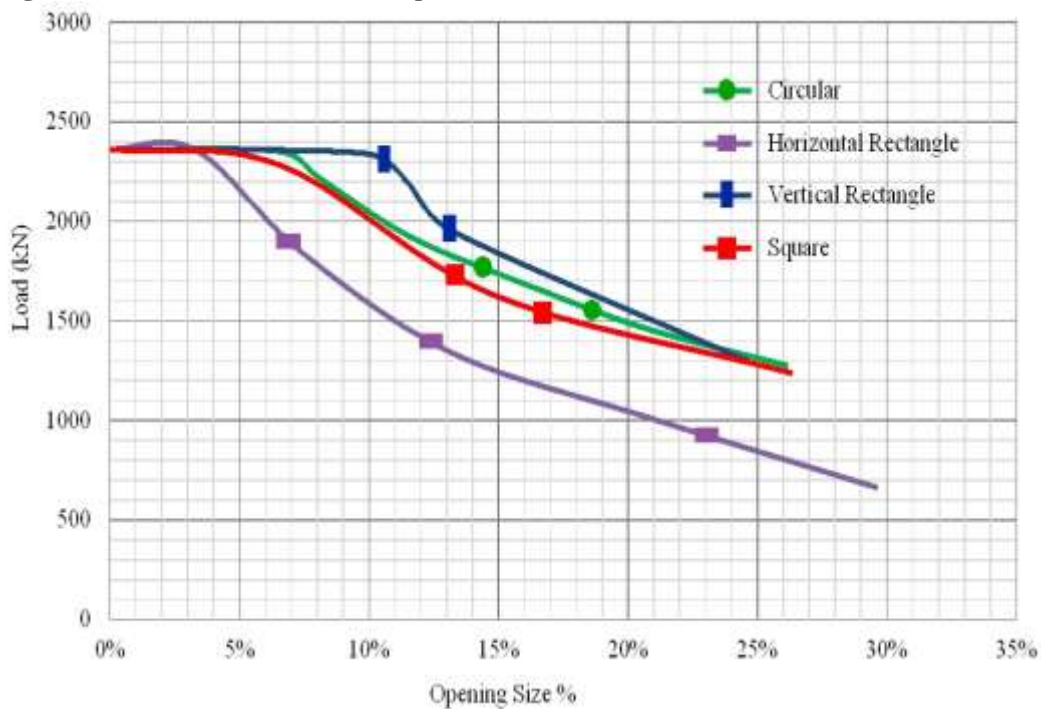
Table 8. *Changing Opening Size Results*

Shape	Opening Position	Opening Area %	Load kN	Capacity reduction than solid wall %	Out of plane displacement (mm)
Solid		0.00%	2363	0.00%	21
Circular (Dia. = 0.45m)	Middle	6.54%	2351.97	0.47%	17.3
Circular (Dia. = 0.50m)	Middle	8.08%	2219.4	6.08%	15.49
Circular (Dia. = 0.60m)	Middle	11.63%	1920.78	18.71%	15.23
Circular (Dia. = 0.70m)	Middle	15.83%	1695.6	28.24%	10.4
Circular (Dia. = 0.80m)	Middle	20.67%	1463.4	38.07%	8.225
Circular (Dia. = 0.90m)	Middle	26.17%	1275.48	46.02%	7.5

Effect of Shear Wall Thickness

Figure 23. *Load - Slenderness Ratio (λ=H/t) Curve*
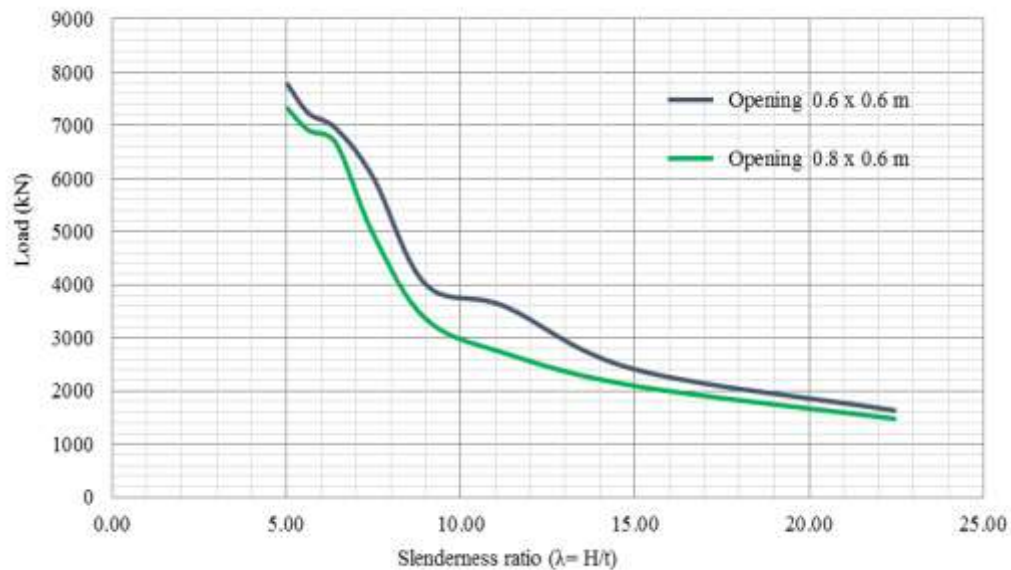
F.E. study is carried out on two different openings in terms of shape and size but both of them locate in the middle of the wall. Each opening is modeled with different wall thicknesses. Figure 23 briefly summarizes results of changing the wall thicknesses where the ultimate axial loads are shown in the vertical axe and slenderness ratio (λ=H/t) are shown in the horizontal axe. The load - slenderness ratio curves indicate that there is a gradual increase in ultimate axial load when slenderness ratio is higher than 10. The graph shows a sharp increase in ultimate axial load when slenderness ratio is lower than 10. Another noticeable feature is that when wall thicknesses are large enough, the

out of plane displacement of the shear wall at failure becomes less and that leads to ductility reduction. According to the Table 9, the out of plane displacement for openings 14.81% & 19.75% went down from 12.02 mm to 0.96mm and from 8.4mm to 0.95mm respectively as we move from ratio 22.5 to 5. In conclusion, increasing the wall thickness has considerable effect on the axial capacity but decreasing the wall ductility.

Table 9. *Changing Shear Wall Thickness for Opening 0.6x0.6m & 0.8x0.6m*

Thickness (m)	Slenderness ratio ($\lambda = H/t$)	Opening 0.6 x 0.6 m		Opening 0.8 x 0.6 m	
		Opening Size 14.81 %		Opening Size 19.75 %	
		Load (kN)	Out of plane Dis. (mm)	Load (kN)	Out of plane Dis. (mm)
0.06	22.50	1630.80	12.02	1475.01	8.40
0.09	15.00	2408.40	6.65	2097.90	5.31
0.12	11.25	3599.64	3.69	2717.28	3.15
0.15	9.00	4006.80	3.20	3358.80	2.97
0.18	7.50	6010.20	1.40	4941.00	1.33
0.21	6.43	6939.00	1.00	6660.90	0.99
0.24	5.63	7236.00	0.97	6912.00	0.95
0.27	5.00	7803.00	0.96	7344.00	0.94

Current Mathematical Design Models for R.C. Walls with Rectangular and Square Openings

Presence of openings in R.C. wall significantly decreases its ultimate load capacity in comparison to the solid wall. There is very limited information in the research literature may be due to the complex failure mechanisms of such elements. Design equations are not provided in the design codes to predict the axial strength of a concrete wall with openings. AS3600 (2009) and EN 1992-1-1 (2004) give a few guidelines, which express that if the walls are restrained on all sides and have an opening with a size under 1/10 of the total wall area, the impacts of this opening on the axial strength can be ignored.

The below mentioned design models are improved by many attempts and include effects of area, location, dimensions and boundary condition:

Saheb and Desayi Model

Saheb and Desayi (1990) had studied the effect of one or two openings, positioned either symmetrically or asymmetrically, and combinations of window or door openings. The equation which is given underneath has been proposed to extend the usefulness of their empirical technique to represent the presence of area and position in an opening.

$$N_{u0} = (k_1 - k_2\alpha_x)N_u \qquad \text{eq. (1)}$$

where N_u is the ultimate load of a panel without openings. The constants k_1 and k_2 were obtained using curve-fitting techniques. Under one way (OW) action this procedure yields $k_1 = 1.25$ and $k_2 = 1.22$, while under two way (TW) action $k_1 = 1.02$ and $k_2 = 1.00$. The effect of the area and position of the opening in the wall is taken into consideration via a dimensionless parameter, α_x, defined from equation 2 and Figure 24.

$$\alpha_x = \frac{A_{0x}}{A_x} + \frac{a}{L} \qquad \text{eq. (2)}$$

where A_{0x} and A_x represent the horizontal wall cross-sectional area of the opening (i.e. $A_{0x} = L_0 t$) and of the solid wall (i.e. $A_x = Lt$), respectively. The term a' is figured concurring to the following equation

$$a' = \frac{0.5L^2 t - L_0 t a_0}{Lt - L_0 t} \qquad \text{eq. (3)}$$

Doh and Fragomeni Model

Doh and Fragomeni (2006) proposed another set of constants for Eq. (1) based on new arrangements of tests on walls with openings under both OW and TW actions. The main difference between this model and the Saheb and Desayi model is: Demonstrate different values for the constants, based on another arrangement of experimental tests. In addition, the constants k_1 and k_2 were obtained using curve-fitting techniques, this time through a larger number of tests. For OW panels this yielded $k_1 = 1.175$ and $k_2 = 1.188$, while for TW panels $k_1 = 1.004$ and $k_2 = 0.933$. Both models take into consideration the area and location of an opening through the parameter α_x, permitting a decrease in the ultimate capacity. Fragomeni et al. (2012) found that this model provides outputs in good agreement with the test results from another experimental study (Lee 2008).

Guan et al. Model

Guan et al. (2010) found that raising both the length and the height of an opening has the most considerable effect on the capacity and proposed a new model in order to take this effect into consideration. Having established a benchmark model, the authors executed a parametric study by changing the parameters that the capacity was most sensitive to. Their analysis proceeded via a nonlinear F.E. approach. In the model a three-dimensional stress state was used with elastic brittle fracture behavior for concrete in tension, and a strain hardening plasticity technique was supposed for concrete in compression. Their model is almost conformable to that proposed by Doh and Fragomeni (2006),

the main contrast being that α_x was changed to α_{xy} to take the opening height into consideration.

$$\alpha_{xy} = \frac{\alpha_x + \gamma \alpha_y}{1 + \gamma} \quad \text{where} \quad \alpha_y = \frac{A_{0y}}{A_y} + \frac{d}{H} \qquad \text{eq. (4)}$$

in which A_{0y} represents the vertical cross-sectional area of the opening (i.e. $A_{0y} = H_0 t$), Ay represents the vertical cross-sectional area of the solid wall (i.e. $A_y = Ht$) and d represents the distance between centers of gravity (G_1 and G_3) of the wall with and without the opening, in the vertical direction (Figure 24). γ represents ''the weighting ratio indicating the percentage of α_y in relation to α_x''. Using regression analysis, a new set of constants was determined; $\gamma = 0.21$, $k_1 = 1.361$ and $k_2 = 1.952$ for OW walls and $\gamma = 0.40$, $k_1 = 1.358$ and $k_2 = 1.795$ for TW walls. It ought to be noted that this model was obtained from walls with an aspect ratio of unity and a fixed slenderness ratio (i.e. k = 30).

Figure 24. *Geometry of a Wall with Openings (G3 = Center of Gravity of Wall with Opening, G1 = Center of Gravity of Solid Wall, G2 = Center of Gravity of Opening)*
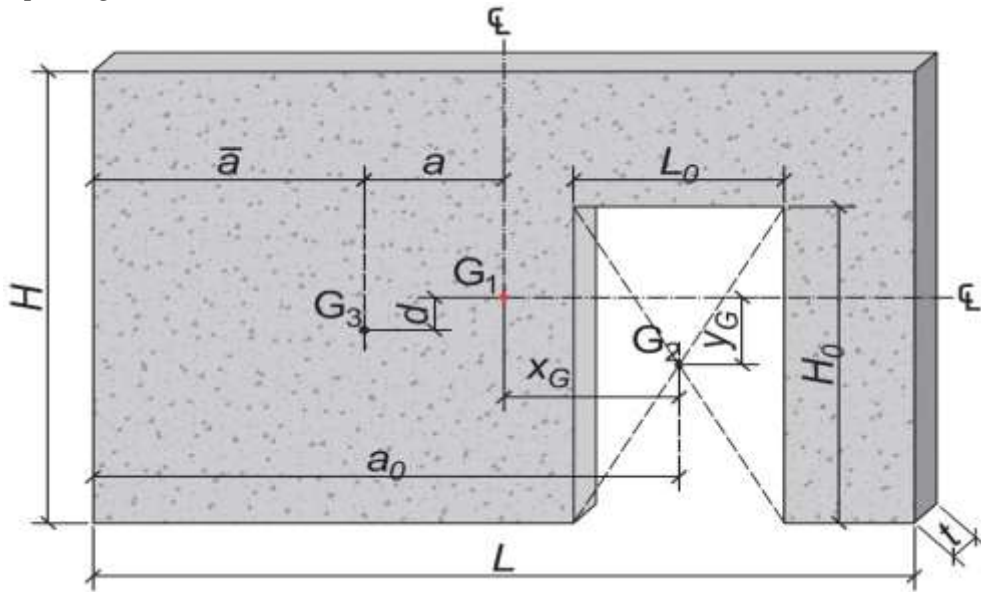
The above-mentioned researchers didn't take into considerations some important parameters which affect the accuracy of these models such as changing the thicknesses of R.C wall with opening, walls with eccentricities above t/6 and the effect of circular openings on R.C. Walls. Therefore, a statistical analysis is performed on each model in turn, using all of the results conducted by the F.E. models available in order to validate the accuracy of the mathematical current design models.

Comparison between the Proposed F.E.M and the Current Mathematical Design Models for R.C. Walls with Rectangular and Square Openings

By using the results of 38 F.E. models, Figure 25 represents the ultimate axial strength of the wall predicted by the F.E. approach versus the ultimate axial strength of the wall predicted by the investigated mathematical design models. The tested walls are assumed to be loaded axially with an eccentricity of t/6. The axial capacity values for F.E. models are close to mathematical axial capacity values conducted by the three mathematical design models. According to the figure, the accuracy varies from -20.8% to +26%. It can be seen that Saheb and Desayi model (1990) and Doh and Fragomeni model (2006) almost provide slightly higher ultimate axial loads than the proposed F.E. model. On the other hand, the ultimate axial loads predicted by Guan et al. model (2010) are approximately very close to the proposed F.E. model. Therefore, the model proposed by Guan et al. (2010) has the best performance relative to the proposed F.E. model.

Figure 25. *Assessment of Ultimate Load Design Models*
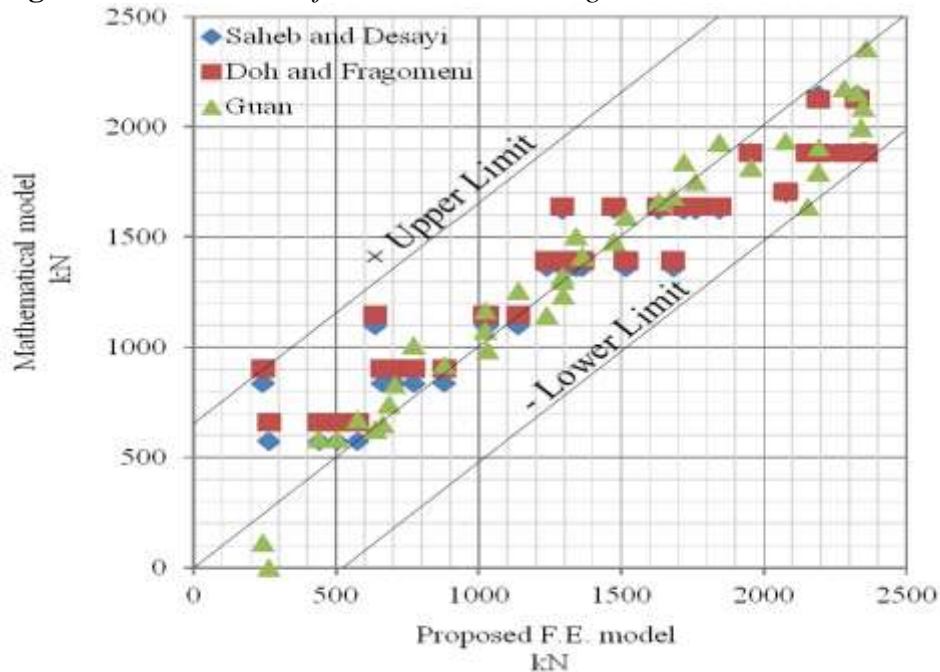
Through the statistical analysis of the proposed F.E. studies, this study indicates areas where further testing is required in order to enhance the reliability of current design models. It was found that most researches have focused on testing RC walls under OW and TW action, with a fixed eccentricity of t/6. Therefore, more tests are required in these experimental regimes to facilitate the development of appropriate design models. Obtaining the mathematical formula of the ultimate axial strength of the R.C. wall with circular opening is studied in this research.

Proposed Model for the Ultimate Axial Strength of the R.C. Wall with Circular Opening

Based on the findings of the F.E. approach and other studied mathematical design models, Figure 26 represents regression analysis results of 5 R.C. wall specimens with different circular openings sizes. These specimens have been tested by ANSYS up to failure and the following formula is proposed using curve-fitting technique for ultimate axial strength of walls with circular opening:

$$N_{uo} = N_u + 165606P^3 - 68518P^2 + 2438.2P$$

Where

N_{uo}: the predicted ultimate load of a R.C. wall with circular opening

N_u: the ultimate load of a R.C. wall without openings

P: the circular opening area percentage from the total wall area

Figure 26. *Load-size Relationship Curve of R.C Wall with Circular Opening*
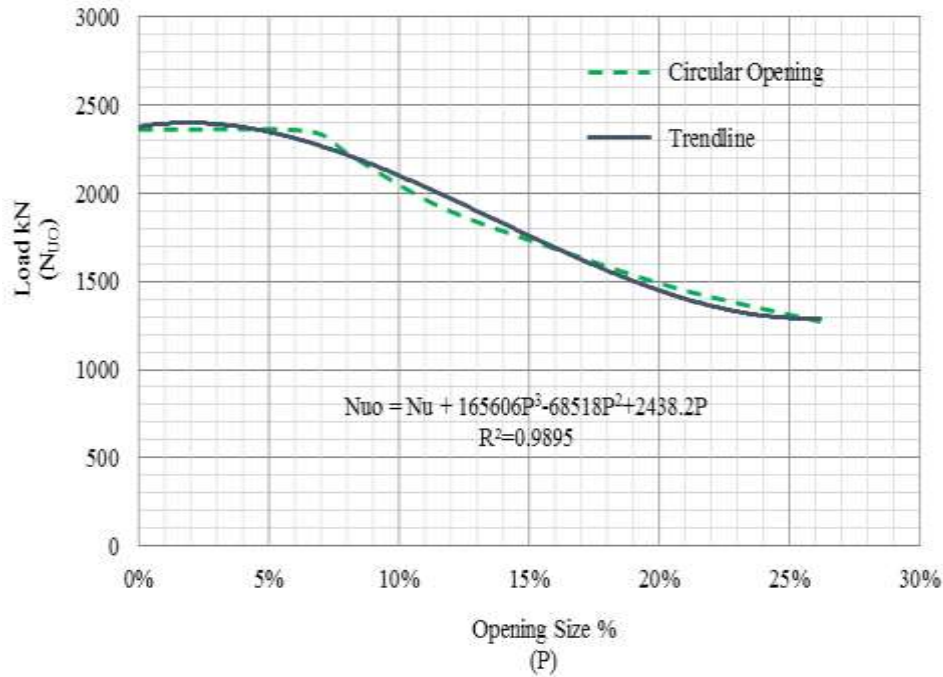
Conclusions

Based on the study presented herein, the following conclusions have been drawn:

- The R.C. wall with vertical rectangle direction opening has the highest axial load capacity compared with square and circular opening which have the same opening size. The main reason is that the loaded cross section area at the opening section in the R.C. wall with vertical

rectangle opening is larger than those in the other shapes at the same opening section. Therefore, this large area can resist higher axial load values. So, the findings indicate that the effect of changing the opening shape should not be ignored.

- Changing the opening orientation has considerable impact on the wall ductility and the axial capacity values as R.C wall with vertical rectangle direction opening has better characteristics than horizontal rectangle direction opening because the loaded cross section area at the opening section in the R.C wall with vertical rectangle opening is larger than the loaded cross section area in the R.C. wall with horizontal rectangle opening at the same opening section.
- Increasing the aspect ratio of horizontal rectangle direction openings in R.C. walls with constant opening size leads to axial capacity reduction because of the reduction in the resisting cross section area in the R.C. wall.
- The optimum opening position in the shear wall regarding axial load capacity is at the lower middle because this position is away from the loaded edge and the axial load path. On the other hand, regarding ductility is at the exact middle of the shear wall.
- R.C. wall with small opening with an area less than 7% of the total have negligible effect on shear wall capacity. In contrast, if the size of the opening is large enough (size >7%), the amount of shear walls capacity and ductility decreases.
- Increasing the wall thickness has considerable effect on the axial capacity but leads to the wall ductility reduction.
- This research studies the gaps of the previous mathematical design models and takes into considerations some important parameters, which affect the accuracy of these models such as changing the thicknesses of R.C. wall with opening, walls with eccentricities above $t/6$ and the effect of circular openings on R.C. Walls.
- Based on the F.E. parametric study, a new mathematical formula has been conducted using curve-fitting technique to predict the ultimate axial strength of R.C. wall with circular opening.

References

ANSYS – Release Version 11. *A Finite Element Computer Software and User Manual for Nonlinear Structural Analysis*. Canonsburg, PA: ANSYS 2007 Inc.

AS3600 (2009) *Concrete Structures*. Sydney, Australia: Standards Australia.

Chowdhury SR, Rahman MA, Islam MJ, Das AK (2012) Effects of Openings in Shear Wall on Seismic Response of Structures. *International Journal of Computer Applications (0975 – 8887)* 59(1).

Doh JH, Fragomeni S (2006) Ultimate Load Formula for Reinforced Concrete Wall Panels with Openings. *Advances in Structural Engineering* 9(1): 103-15.

EN1992-1-1 (2004) *Eurocode 2: Design of Concrete Structures – Part 1–1: General Rules and Rules for Buildings.* Brussels: COMITE EUROPEEN DE NORMALISATION.

Fragomeni S, Doh JH, Lee DJ (2012) Behavior of Axially Loaded Concrete Wall Panels with Openings: An Experimental Study. *Advances in Structural Engineering* 15(8): 1345-58.

Guan H, Cooper C, Lee D-J (2010) Ultimate Strength Analysis of Normal and High Strength Concrete Wall Panels with Varying Opening Configurations. *Engineering Structures* 32(5):1341-55.

Kankuntla A, Sangave P, Chavan R (2016) Effects of Openings in Shear Wall. *IOSR Journal of Mechanical and Civil Engineering (IOSR-JMCE)* 13(1): 1-6.

Kwan AKH, Dai H, Cheung YK (1999) Non-Linear Sesimic Responce of Reinforced Concrete Slit Shear Walls. *Journal of Sound and Vibration* 226(4): 701-718.

Lee D-J (2008) *Experimental and Theoretical Study of Normal and High Strength Concrete Wall Panels with Openings*. PhD Thesis. Australia: Griffith University.

Lin CY, Kuo CL (1988) Behaviour of Shear Wall with Opening. *Ninth World Conference on Earthquake Engineering in Tokyo.*

Mohammed BS, Ean LW, Anwar Hossain KM (2010) CFRP Composites for Strengthening of Reinforced Concrete Walls with Openings. *International Journal of Engineering Research and Applications* 1(4): 1841-1852.

Morsy AM, Helmi KM, El-Ashkar NH, Nada M (2015) Flexural Strengthening for R.C. Beams using CFRP Sheets with Different Bonding. *International Conference on Advances in Structural and Geotechnical Engineering in Hurghada.*

Mosoarca M. (2014) Failure Analysis of RC Shear Walls with Staggered Openings under Seismic Loads. *Engineering Failure Analysis* 41(0): 48-64.

Musmar MA (2013) Analysis of Shear Wall with Openings Using Solid65 Element. *Jordan Journal of Civil Engineering* 7(2).

Popescu C, Sas G, Sabău C, Blanksvärd T (2016) Effect of Cut-Out Openings on the Axial Strength of Concrete Walls. *Journal of Structural Engineering* 142(11).

Rusch H, Hilsdorf HK (1963) *Deformation Characteristics of Concrete under Axial Tension*. Munich: Voruntersuchungen, Bericht 44.

Saheb SM, Desayi P (1990) Ultimate Strength of RC Wall Panels with Openings. *Journal of Structural Engineering* 116(6): 1565-78.

Terec L, Bugnariu T, Păstrav M (2010) Analiza Neliniară a Cadrelor din Beton Armat cu Pereți Turnați în Situ. [Non-Linear Analysis of In-Concrete Wall Armed Buildings.] *Romanian Journal of Materials* 40(3): 214-221.

William K.J, Warnke EP (1975) Constitutive Model for the Triaxial Behavior of Concrete. *Proceedings of the Int. Assoc. Bridge Struct. Eng. Sem. Concr. Struct.* 19, 1-31. Bergamo, Italy.

An Exploratory Study of the Role of the Human Resource Information System Professional

By Sapora Bradley[*]

The increasing implementation of technology applications into the workplace has substantiated the need for adept professionals who can manage HR technology for employees and provide data about the organization. For some companies, these professionals are found within the human resources department. These information systems professionals combine HR knowledge and technology skills to provide applications that improve work processes and HR outcomes. This qualitative study focused on exploring the role delineation of human resource information systems (HRIS) professionals to better understand the advantageous aspects of the role's focus in HR technology and analytics. Specifically, the study aimed to describe how the HRIS professional role supports the functions of HR and transformation of HR activities within organizations. Additionally, the research sought to uncover how HRIS professionals described their responsibilities and competencies in response to the significance of data analytics, as well as how the HRIS professionals described the outlook of their professional role. Ten, semi-structured interviews were conducted with HRIS professionals who reported having progressive HRIS experience within U.S. based organizations. The results included HRIS professionals' beliefs about their tasks, competencies, and job outlook and thematic analysis resulted in six categories: data management, HR/IT intersection, HRIS emergence, business intelligence, professional identity, and job satisfaction. The conclusions drawn from the research findings indicated that: HRIS professionals encourage HR technology integration to improve workplace processes; HRIS professionals manage data integrity and support the safeguarding of employee information; HRIS professionals run data inquiries and provide reports that influence decision making related to workforce and business outcomes; and HRIS professionals are enthusiastic about emergent job responsibilities in the design and coding of systems.

Keywords: *Employee Data Management, Human Resource Information Systems, Human Resources, Role Delineation.*

Introduction

With technology usage increasing and an influx of digital natives in the workforce, organizations are met with increasing demands to consider how to incorporate and manage technology applications for their employees (Bersin, 2016; Sierra-Cedar, 2016). In an increasingly competitive and complex business environment, HR technology has been promoted as a solution to simplifying work and cutting data complexity through improved systems (Weeks, 2013). As evolving technology and emerging best practices in workplace processes continue to transform organizations, HRIS professionals hold a unique positioning at the intersection of understanding HR functions and technology solutions. A survey of 32,000 HR professionals, leading to the report on Human Resources Competency

[*]Researcher, Pepperdine University, USA.

(SHRM, 2012), found that although being a proponent of technology was considered a desirable trait, the perceived impact on HR effectiveness and the perceived impact of technology on business performance were low. Additionally, the report on Global Human Capital Trends revealed little urgency among respondents concerning the adoption of HR technology (Deloitte Consulting, 2014). The intersection between IT and HR can pose problems when IT is not invested as stakeholders in HR software solutions. To earn support from executives and other functional areas, a demonstrated need must occur concerning the role of HRIS and its importance. When HR is unable to defend a technological business strategy with metrics and analytics investment is denied and allocated to other departments within the organizational (Higgins, 2014).

A crucial assumption about this study is the need to have HR technology managed by the HR function rather than the IT function. This stance is based on the researcher's own experience at organizations without dedicated HRIS staff, where technology solutions were heavily influenced by IT workload and stake in new projects. It is therefore assumed that technology is at the intersection of IT and HR, signaling that a difference exists concerning the perceived importance of human capital management (HCM). This study also assumes that HRIS is a necessary component for all organizations regardless of size and industry. It was the researcher's intent to utilize the research data to uncover professional opinions about how the participants are applying HRIS principles within various organizational landscapes.

To understand the trajectory of the HRIS professional and establishment within organizations this study posed a central guiding question and two sub-questions:

- How does the HRIS professional role support the functions of HR and transformation of HR activities within organizations?
- How do HRIS professionals describe the responsibilities and competencies of the role in response to the emergence of big data?
- How do HRIS professionals describe the outlook of their professional role within organizations and the HR profession?

To examine the HRIS professional role, two concepts were considered when analyzing the research data. Organizational role theory and delineation describes how employees define their role and how other professionals respond to such definitions (Naikar, 2013; Prien, 2009). Additionally, the study considered HCM theory and the contribution of HRIS professionals to an organization's competitive advantage. The HCM theory also assesses how HR technology influences the management of the HR functions (Sierra-Cedar, 2014).

Literature Review

The topic of HRIS solutions is most often found within e-human resource management (HRM) literature, where these systems are considered a tool for HR

departments. Martinsons (1997) had defined HRIS as consisting of sophisticated information technology tools which improve HR processes and contributes to the quality of human capital within organizations. Hendrickson (2003) expands and identifies HRIS as more than the use of software but a system inclusive of technology, end-users, data, and policies. Bondarouk et al. (2009) described an HRIS as providing multiple services covering three main functions: operations of daily transactions, relational communication between stakeholders, and transformational decision making.

Mayfield et al. (2003) stipulate that the goal of an HRIS is to harness technology as a tool which can lower barriers to HR's strategic efforts. Different activities, such as solutions for recruiting, payroll, and self-service are therefore undertaken with a new emphasis on technology as many of these transactional activities have been characterized as ideal for automation (Bersin, 2017). By automating the operational, HR departments leverage technology in order to free up resources to do other, more strategic work.

Lepak and Snell (1998) characterized HRIS software as being a relational database for stakeholders, where information is collected and then shared between other functional departments within the organization. Firestone and McElroy (2003) explained that this intra-organizational communication of data represents double-loop learning and feedback as individuals continuously draw conclusions from beliefs, actions, and reactions that are occurring within the organization. While Casalino et al. (2015) described the success of systems implementations as being influenced by paths to organizational learning.

Research reveals a chasm between the potential proposed by HRIS adoption and the actual success of enterprise-wide HRIS (Tansley and Watson, 2000). In addition to challenges related to investment and resource allocation, criticism about HRIS may contribute to difficulty in solution integration. These criticisms include the belief that operational efficiencies should be attributed to IT departments and not to HR departments, as well as a belief that HR departments benefit from automation service, while other departments within an organization see little direct value (Martinsons, 1997; Panayotopoulou et al., 2010; Strohmeier, 2007). However, it is ideal for HR, IT, and business departments to work together when evaluating and appraising existing HCM procedures and the integration of HRIS solutions.

Concerning technology adoption among employees, literature addresses an organization's need to innovate or perish. Organizational behavior theories indicate strong responses to external threat factors within the business landscape that results from vendor promotion, government policies, and competitive pressure within the industry (Silverstein et al., 2012). Cummings and Worley (2015) attributed the response to transformation and rate of change as being dependent upon both internal and external factors that are imposed on the organization. Guzmán-Cuevas, Cáceres-Carrasco, and Soriano (2009) attributed innovation to a dependency on current economic conditions. Brynjolfsson and McAfee (2014) address an organization's IT investment as a leading factor for business management innovation.

Factors for implementing technology innovation will be specific to the individual organization. The technology acceptance model indicates that the perceptions of usefulness and ease of use are the determinants of technology adoption among organizational employees (Davis, 1989). Similarly, perceived effort and time to learn new technologies affected adoption among employees (Goodman and Darr, 1998). Kim and Lee (2006) also supported the ease of use factor and suggested the importance of a culture of acceptance. Overall, the value of an HR technology product will be determined by the practitioners and end-users. The gap in technology adoption is also influenced by the perceived costs of implementation (Moore, 1999; Smolcic et al., 2014).

Bell et al. (2006) discussed the influence IT departments have concerning HR's technology transformation. However, literature is lacking in research related to the adoption of specific HRIS infrastructure. There are publications about how a new system becomes implemented within a particular organization, but there is little guidance about who should lead, maintain, and be a part of the drive for future HR innovations to keep up with continuously evolving technologies.

A review of HRIS job postings retrieved from LinkedIn and SHRM revealed several key characteristics related to technical complexity, innovation, and autonomy. Concerning the administrative function, HRIS professionals are in charge of collecting data and maintaining it in standardized formats. With respect to project management, HRIS professionals are tasked with preparing upgrades and enhancements to HRM systems, leading user testing, and making recommendations for technology policies. Responsibilities surrounding analytics encompass evaluating workflows for improvement opportunities, running queries and reports for the business function, and utilizing mathematical models to interpret raw data and make predictions about human capital needs (Dussert, 2014). A survey by the Information Services Group sought to identify goals of HRIS managers in various organizations. Objectives included speedy implementation of new systems, improved user experience with technology, and identification of data shortfalls in the current organizational design (Sivak and Card, 2014).

Methodology

Based on the limited foundational research about HRIS professionals, this study utilized an exploratory approach to inquiry. Stebbins (2001) defines exploratory research as an effort to more thoroughly explain an idea or observation from the standpoint of the target population's attitudes, opinions, and behavior associated with the topic. This type of research is conducted before engaging in qualifying research that generalizes findings. This exploratory study utilized the qualitative research technique of interviewing. Recruitment and purposive sampling stipulated that participants have seven years of progressive work experience dedicated to the HRIS specialty, work at a U.S. based enterprise, and preferably hold a higher education degree in HR or IT. Organization size and industry were expected to be varied as participants were anticipated to share their

experiences within HRIS before their current job role, thus having occurred across numerous organizations. The researcher believed that experienced professionals could speak to fluctuating workforce trends and demands for technology in the workplace. Ten HRIS professionals participated in interviews with the researcher. Although this study did not seek a statistically representative sample, the use of experts contributed to the credibility of the study results. According to Gobet's (2016) definition, an expert is an individual having knowledge and experience of the topic being discussed.

Prior to beginning the interview, the researcher and interviewee discussed the IRB approved informed consent form and the researcher answered any questions that the interviewee had about the study or interview process, including confidentially concerns. Interviews were conducted by phone or FaceTime and lasted between 45-55 minutes. The logistics and feasibility of the study were tested with a pilot study conducted with two HRIS professionals who met the criteria of the sample population.

The researcher followed a semi-structured interview protocol and inquired about their educational backgrounds, employment history, and professional development. The participants also responded to questions about their entry into the specialty, their job responsibilities, and their opinions about HRIS in the workplace. To confirm the internal validity of the interview approach, interview questions posed by the researcher were first examined by a professional familiar with HRIS topics and interview protocol.

The interviews were audio recorded and then transcribed using HyperTRANSCRIBE, an audio transcription tool. The researcher also took detailed handwritten notes and memos to capture other specifics that occur during the interview such as making notations about tone, body language, or implications that are not easily gleaned from the audio recordings alone. Kvale and Brinkman (2009) noted that other information in addition to the words spoken can be found within the interview. It is the researcher's task to determine the full message being expressed by the participant and to capture those impressions within the moment.

A system was developed by the researcher to code interview responses. These codes were used to determine patterns in the data, identify themes, and comprehend the overarching connections across categories (Charmaz and Belgrave, 2012; Creswell, 2013). Each interview then received an in-depth review by the researcher. This focused reading familiarized the researcher with the data in an attempt at identifying all possible coding opportunities. The researcher also used qualitative research software, HyperRESEARCH, to organize data and codes from the interviews. After the basic coding, more interpretive coding occurred to engage in thematic and narrative analysis related to the participant's opinions, personal experiences, and perceptions. The researcher conferred with a peer reviewer who evaluated the researcher's coding scheme and examined the consistency of the coding. The researcher and peer reviewer also discussed appropriate changes to the codebook.

Results

Table 1 lists the participants by code and includes number of years within the HRIS specialty and current business industry.

Table 1. *Interviewee Demographics*

Participant Code	Time as HRIS Professional	Current Industry
3Z2	14 years	Technology
6MF	5 years	Education
7N7	20 years	Education
CTG	18 years	Healthcare
EH8	7 years	Education
PC9	8 years	Healthcare
T3U	9 years	Energy
V68	38 years	Education
XGE	10 years	Consulting
ZWU	7 years	Education

The exploratory nature of the design provided an extensive amount of data. The qualitative analysis of the interviews resulted in 724 coded passages grouped into six categories (a) data management, (b) HR/IT intersection, (c) HRIS emergence, (d) business intelligence, (e) professional identity, and (f) job satisfaction. Table 2 lists the six categories with themes and counts. Additional sub-themes were identified and aided the researcher during data analysis.

Table 2. *Thematic Categories*

Category	Theme	Count
Data Management	Curation	51
	Ownership	19
	Resources	72
HR/IT Intersection	Structure	45
	Task Allocation	26
HRIS Emergence	Culture	26
	Career Outlook	23
	Technology	55
Business Intelligence	Data Leverage	13
	Insights	28
	Reporting	30
Professional Identity	Education	15
	Job Role	81
	Motivations	37
	Perceptions	88
	Previous Experience	41
	Professional Development	48
Job Satisfaction	Factors	26

Note: N = 724 coded passages.

Discussion of Key Findings

Participants spoke to the emergence of HRIS in response to industry norms and organizational culture. Many associated the growth of HRIS with the usage of technology by employees and the collection of employee data. In general, participants stated that HRIS emergence was a direct response to technology trends. The data implied that there was a generational difference, where younger employees were more adapt with technology, but would become frustrated with certain limitations. Other generations appeared to place more responsibility on the HRIS professionals and had a more difficult time adapting to new work processes.

Participants described data management concerns, including data integrity, compliance, and moving away from paper collection methods toward more simplified digital capturing. Attention was given to the ownership of data as related to how information was stored, made available, and disseminated to the appropriate parties. A concern about storing data in-house versus the cloud presented itself among participants who suggested that it was useful for certain sized organizations, but at the cost of losing some amount of control over the data. Participants also described application and enterprise development, customization, and the cost-benefit comparison to homegrown resources.

HRIS professionals discussed their organization and departmental structures, including sizes of organizations they had worked at and how implementation projects were staffed. In some cases, the HRIS professional was classified under the IT department. There were also instances where organizations did not have an IT resource in-house. Participants considered task allocation between HRIS and IT professionals and classified tasks that were distinct to each role.

Participants described executive interest in data leverage and provided examples of desired employee outcomes. Participants spoke considerably about report pulling, including creating their own custom reports, using reports from vendor applications, and combining reports. Most participants believed that their organizations embraced metrics but indicated that their organizations fell short of utilizing data reports to produce predictive outcomes. The consensus seemed to be that organizations were not actively developing analytic models.

Conclusions and Implications

The first conclusion states that HRIS professionals encourage HR technology integration to improve workplace processes by disrupting outdated and inefficient manual processes within the workplace. The HRIS professionals interviewed are knowledgeable about processes, organizational data, and technology trends. Participants described their efforts in researching and vetting HRIS applications and systems for implementation into their organizations. Much of their time was dedicated to meeting with end users and seeking the best solutions to improve their day-to-day activities. This conclusion considers HRIS professionals as HR technology experts, seeking a balance between knowledge and application (Stokes, 1997). HRIS professionals benefit from actively engaging in the specialty

by seeking professional certifications, attending conferences, and communicating with their personal learning networks to expand their knowledge. This finding supports Bailey (2015) whose phenomenological study revealed that professional development is part of the HR practice and that non-formal learning is experienced as a means of professional development. The study participants demonstrated that successful HRIS professionals are problem-solvers and systematic and analytical thinkers.

The second conclusion states that HRIS professionals manage data integrity and the gatekeeping of employee information. HRIS helps organizations with complex employee classifications, and therefore complex data. Participants described the influx of employee data and the need to confirm correct information about employees, comply with retention laws, and oversee the access and dissemination of employee information and workforce data shared within the organization. This finding considers role theory, as several of the professionals interviewed described that the crossover of HRIS and IT raised questions about the boundaries related to where responsibility lies with HRIS applications and systems, and employee data. As noted by Stamper and Johlke (2003) organizations consider role theory by addressing role conflict and role ambiguity. Additionally, some participants attested to collaborative efforts with other departments as being positive experiences, whereas others had experienced instances where there was lack of engagement. Therefore, conflicts can be lessened by engaging in reoccurring meetings, collaborative projects, and embracing opportunities for knowledge transfer. These findings support the work of Cerra et al. (2013) who concluded that collaboration was a means of navigating organizational politics. Collaborative engagement can, therefore, improve the relationship between HR and IT departments concerning systems implementations.

The third conclusion states that HRIS professionals run data inquiries and provide reports that influence decision making related to workforce and business outcomes. Participants revealed that pulling reports and data mining was a significant feature of their role. Participants described the various requests for metrics concerning employee data and human capital figures that were requested by executives and other leaders. HRIS professionals were adept at making customized reports by combining several reports into one. This was essential when the participants concluded that a customized report would contribute to a better narrative for the requestor. Literature indicates that knowledge of metrics and analytics lead to actionable insights and therefore improved business outcomes (Weisbeck, 2016). SHRM (2012) identified technology usage as a means to solve business problems as a competency related to business acumen. For HR departments, the reporting of metrics and further consideration of analytics becomes an essential component that moves the HR function from operational to strategic tasks. As suggested by the HCM theory, HR then becomes an asset by improving business outcomes and talent appraisal (National Academies of Sciences, Engineering, and Medicine, 2017; Sierra-Cedar, 2014). Therefore, HRIS' reporting responsibilities support outcomes of various HR functions, such as recruiting, training, compensation and benefits, and succession planning.

However, the HRIS professionals agreed that big data analytics to make predictions was emerging but consequently underutilized in the workplace.

The fourth conclusion states that HRIS professionals are enthusiastic about emergent job responsibilities in HRIS system design and coding. Participants described basic coding that they utilize during system implementations and upgrades. Respondents enjoyed the challenging nature of combining HR knowledge and people skills with technology solutions. HRIS professionals discussed workarounds and customizations that they aimed to complete for end users. Additionally, HRIS professionals expressed interest in gaining more education in IT specific areas and some had already sought system certifications from product vendors that they are currently using in-house. Several HRIS professionals insisted that they identified as technology professionals and as having a knack for technology. There were also opportunities for HRIS professionals to make lateral movements into IT. These results also concern role theory as it relates to professional identify and self-identification of the participants as being tech savvy (Walsh and Gordon, 2008). These findings support the work of Lawler and Boudreau (2015) whose yearly surveys indicated increased satisfaction among HR professionals with utilizing technical skills. Therefore, these new skills also contribute to contentment and satisfaction among HRIS professionals.

Practice and research related recommendations emerged from the data. Interview participants described resistant attitudes from end users, suggesting that HRIS professionals needed to gain stakeholder confidence. Mondare et al. (2011) discussed the importance of executive buy-in. As mentioned by the participants, individuals in leadership positions typically recognized the value of HRIS. Therefore, leaders and executives can influence the opinions of end users as to the helpfulness and credibility of HRIS professionals by expressing buy-in, in a way that is visible and impactful on the culture of the organization. This could potentially encourage better working relationships between HRIS professionals and end users.

Given that some participants described their organizations as not using HR analytics, it is recommended that companies lacking in data analytics consider developing an organizational analytics team that makes use of data within the organization and develops analytic models. Roles on this team would include a project manager, business analyst, and database administrator (EMC Education Services, 2015). In this capacity, HRIS professionals would play a significant role in developing measures for big data analytics. HRIS professionals would be unique contributors to an analytics team, because they are very familiar with people data and can represent the interests of the HR department.

The interviews also revealed opportunities for additional research. With participants discussing the cost savings associated with the adoption of cloud-based systems and the outsourcing of the IT function, it is recommended that research is conducted concerning this trend. Specifically, how this trend might reveal information about the development of new HRIS skills in coding and system management in organizations. Research can be specific to industry and organization size in demonstrating the consolidation of responsibilities.

The sample focused on HRIS professionals with seven years of progressive HRIS experience in U.S. based organizations. The recruitment parameters did not reflect the youngest generation in the workforce. As the workforce is nearing a changing tide concerning preparation and technology fluency, there probably are insights into the proclivity for technology and the self-identification of the upcoming HRIS leaders and their end users that these professionals' views did not address.

Closing Remarks

This study involved HRIS professionals of various titles and from various industries. This produced extensive amounts of data, which was helpful in the board, exploratory sense however industry specific or role specific conclusions cannot be made. Researcher bias was considered, as the researcher was interested in this topic because of previous work experience in both the HR and IT departments. To convey accurate interpretation to the reader, the researcher engaged in reflexivity throughout the study including validation and pilot testing of the interview questions. Multiple reviews and coding of interview transcripts occurred, and a peer reviewer was recruited to ensure consistency of the interpretation of the interview data.

The study provided an in-depth analysis of the preparation and responsibilities of HRIS professionals and comments on the outlook for the profession. The results of this study confirmed that HRIS professionals help improve work processes by procuring useful applications for employees. Additionally, HRIS professionals can contribute to HR's strategic positioning within organizations by reporting actionable insights and thus encouraging the movement toward predictive analytics.

References

Bailey, M. (2015). Professional development of HR practitioners: A phenomenographic study. *European Journal of Training and Development, 39*(3), 220-238. Doi: 10.11 08/EJTD-08-2014-0057.

Bell, B., Lee, S., Yeung, S. (2006). The impact of e-HR on professional competence in HRM: Implications for the development of HR professionals. *Human Resource Management, 45*(3), 295-308. Doi: 10.1002/hrm.20113.

Bersin, J. (2016). *Predictions for 2017: Everything is becoming digital*. Retrieved from https://www2.deloitte.com/content/dam/Deloitte/at/Documents/about-deloitte/predi ctions-for-2017-final.pdf.

Bersin, J. (2017). Transformative Tech: A disruptive year ahead. *HR Magazine, 62*(1), 28-36. Retrieved from https://www.shrm.org/hr-today/news/hr-magazine.

Bondarouk, T., Ruël, H. and van der Heijden, H. (2009). e-HRM effectiveness in a public sector organization: A multi-stakeholder perspective. *The International Journal of Human Resource Management, 20*(3), 578-590. Doi: 10.1080/09585190802707359.

Brynjolfsson, E. and McAfee, A. (2014). *The second machine age: Work, progress, and prosperity in a time of brilliant technologies*. New York, NY: Norton & Company.

Casalino, N., Cavallari, M., DeMarco, M., Ferrara, M., Gatti, M. and Rossignoli, C. (2015). Performance management and innovative human resource training through flexible production systems aimed at enhancing the competitiveness of SMEs. *The IUP Journal of Knowledge Management*, *13*(4), 29-42. Retrieved from http://www. iupindia.in/Knowledge_Management.asp.

Cerra, A., Easterwood, K. and Power, J. (2013). *Transforming business: Big data, mobility, and globalization*. Indianapolis, IN: Wiley.

Charmaz, K. and Belgrave, L.L. (2012). Qualitative interviewing and grounded theory analysis. In J. F. Gubrium, J. A. Holstein, A. B. Marvasti and K. D. McKinney (Eds.), *The SAGE handbook of interview research: The complexity of the craft* (pp. 347-366). Thousand Oaks, CA: SAGE Publications.

Creswell, J. W. (2013). *Qualitative inquiry and research design: Choosing among five approaches*. Los Angeles, CA: SAGE Publications, Inc.

Cummings, T. G. and Worley, C. G. (2015). *Organization development & change*. Stamford, CT: Cengage Learning.

Davis, F. D. (1989). Perceived usefulness, perceived ease of use, and user acceptance of information technology. *MIS Quarterly, 13*(3), 319-340. Retrieved from http://www. misq.org.

Deloitte Consulting. (2014). *Global human capital trends 2014: Engaging the 21-century workforce*. Retrieved from https://bit.ly/2o2GhQO.

Dussert, B. (2014). HR should hire 'scary' data people. *Forbes.* Retrieved from http://www. forbes.com.

EMC Education Services. (2015). *Data science and big data analytics: Discovering, analyzing, visualizing and presenting data*. Indianapolis, IN: Wiley.

Firestone, J. M. and McElroy, M. W. (2003). *Key issues in the new knowledge management*. Boston, MA: Butterworth-Heinemann.

Gobet, F. (2016). *Understanding expertise: A multi-disciplinary approach*. London, UK: Palgrave Macmillan.

Goodman, P. S. and Darr, E. D. (1998). Computer-aided systems and communities: Mechanisms for organizational learning in distributed environments. *MIS Quarterly, 22*(4), 417-440. Retrieved from http://www.misq.org.

Guzmán-Cuevas, J., Cáceres-Carrasco, R., & Soriano, D. (2009). Functional dependence and productive dependence of SMEs. *Small Business Economics, 32*(3), 317-330. Doi: 10.1007/s11187-008-9115-0.

Hendrickson, A. R. (2003). Human resource information systems: Backbone technology of contemporary human resources. *Journal of Labor Research, 24*(3), 381-394. Retrieved from https://link.springer.com/journal/12122.

Higgins, J. (2014, November). Bringing HR and finance together with analytics. *HR Magazine, 59*(11), 44-46. Retrieved from https://www.shrm.org/hr-today/news/hr-magazine.

Kim, S. and Lee, H. (2006). The impact of organizational context and information technology on employee knowledge-sharing capabilities. *Public Administration Review, 66*(3), 370-385. Doi: 10.1111/j.1540-6210.2006.00595.x.

Kvale, S. and Brinkman, S. (2009). *Interviews: Learning the craft of qualitative research interviewing* (2nd ed.). Thousand Oaks, CA: Sage Publications.

Lawler, III, E. E. and Boudreau, J. W. (2015). *Global trends in human resource management: A twenty-year analysis*. Stanford, CA: Stanford University Press.

Lepak, D. P. and Snell, S. A. (1998). Virtual HR: Strategic human resource management in the 21st century. *Human Resource Management Review, 8*(3), 215-234. Retrieved from https://www.journals.elsevier.com/Human-Resource-Management-Review.

Martinsons, M. G. (1997). Human resource management applications of knowledge-based systems. *International Journal of Information Management, 17*(1), 35-53. doi: 10.1016/S0268-4012(96)00041-2.

Mayfield, M., Mayfield, J. and Lunce, S. (2003). Human resource information systems: A review and model development. *Advances in Competitiveness Research, 11*(1), 139-152. Retrieved from https://bit.ly/2zutq19.

Mondare, S., Douthitt, S. and Carson, M. (2011). Maximizing the impact and effectiveness of HR analytics to drive business outcomes. *People & Strategy, 34*(2), 20-27. Retrieved from http://www.hrps.org/?page=PeopleStrategy.

Moore, G. A. (1999). *Crossing the chasm: Marketing and selling high-tech products to mainstream customers*. New York, NY: Harper Business.

Naikar, N. (2013). *Work domain analysis: Concepts, guidelines, and cases*. Boca Raton, FL: CRC Press.

National Academies of Sciences, Engineering, and Medicine. (2017). *Information technology and the U.S. workforce: Where are we and where do we go from here?* Doi:10.17226/24649.

Panayotopoulou, L., Galanaki, E. and Papalexandris, N. (2010). Adoption of electronic systems in HRM: Is national background of the firm relevant? *New Technology, Work and Employment, 25*(3), 253-269. Doi: 10.1111/j.1468-005X.2010.00252.

Prien, E. P. (2009). *A practical guide to job analysis*. San Francisco, CA: Pfeiffer.

SHRM. (2012). *Content validation study of the SHRM competency model*. Retrieved from https://bit.ly/2zxWlRN.

Sierra-Cedar. (2014). *HR systems survey white paper, 17th annual* edition. [White paper]. Retrieved from https://www.sierra-cedar.com/research/publications.

Sierra-Cedar. (2016). *HR systems survey white paper, 19th annual edition.* [White paper]. Retrieved from https://www.sierra-cedar.com/research/publications.

Silverstein, D., Samuel, P. and DeCarlo, N. (2012). *The innovator's toolkit: 50+ techniques for predictable and sustainable organic growth*. Hoboken, N.J: John Wiley & Sons.

Sivak, M. and Card, D. (2014). *Human resources technology and service delivery trends in 2014.* [Executive Summary]. Retrieved from http://info.isg-one.com/2014-HR-Technology-and-Service-Delivery.html.

Smolcic, N., Thomas, B. and Contacos-Sawyer, J. (2014). The advantages and affordability of human resource information system's (HRIS) implementation in the small business sector. *Competition Forum, 12*(2), 8-15. Retrieved from http://www.eberly.iup.edu/ASCWeb/journals_cf.html.

Stamper, C. L. and Johlke, M. C. (2003). The impact of perceived organizational support on the relationship between boundary spanner role stress and work outcomes. *Journal of Management, 29*(4), 569-588. Doi: 10.1016/S0149-2063(03)00025-4.

Stebbins, R. A. (2001). *Exploratory research in the social sciences*. Thousand Oaks, CA: SAGE Publications.

Stokes, D. E. (1997). *Pasteur's quadrant: Basic science and technological innovation*. Washington, DC: The Brookings Institution.

Strohmeier, S. (2007). Research in e-HRM: Review and implications. *Human Resource Management Review, 17*(1), 19-37. Doi: 10.1016/j.hrmr.2006.11.002.

Tansley, C. and Watson, T. (2000). Strategic exchange in the development of human resource information systems (HRIS). *New Technology, Work & Employment, 15*(2), 108-122. Retrieved from https://bit.ly/1V0fuD0.

Walsh, K. and Gordon, J. R. (2008). Creating an individual work identity. *Human Resource Management Review, 18*(1), 46-61. Doi: 10.1016/j.hrmr.2007.09.001.

Weeks, K. O. (2013). An analysis of human resource information systems impact on employees. *Journal of Management Policy & Practice, 14*(3), 35-49 Retrieved from http://www.na-businesspress.com/JMPP/WeeksKO_Web14_3_.pdf.

Weisbeck, D. (2016). *Why connecting workforce outcomes to business outcomes matters.* Retrieved from https://bit.ly/2QlAq7v.